NOISE AND CURRENT-VOLTAGE CHARACTERISTICS
OF NEAR-BALLISTIC GaAs DEVICES

By

ROBERT ROY SCHMIDT

A DISSERTATION PRESENTED TO THE GRADUATE COUNCIL OF
THE UNIVERSITY OF FLORIDA
IN PARTIAL FULFILLMENT OF THE REQUIREMENTS FOR THE
DEGREE OF DOCTOR OF PHILOSOPHY

UNIVERSITY OF FLORIDA

1983

ACKNOWLEDGMENTS

TABLE OF CONTENTS

iii

Abstract of Dissertation Presented to the Graduate Council
of the University of Florida in Partial Fulfillment of the
Requirements for the Degree of Doctor of Philosophy

NOISE AND CURRENT-VOLTAGE CHARACTERISTICS
OF NEAR-BALLISTIC GaAs DEVICES

By

Robert Roy Schmidt

April 1983

Chairperson: C. M. Van Vliet
Major Department: Electrical Engineering

Conduction processes in novel submicron $n^+n^-n^+$ and $n^+p^-n^+$ mesa
structures in GaAs are investigated. The widths of the n-type and p-
type layers are 0.4 μm and 0.47 μm, respectively. These small devices
are of interest due to the possibility of ballistic (collision free)
transport which leads to picosecond switching times at femtojoule
power levels, since the velocities of the carriers may be much greater
than the collision-limited drift velocity.

Three noise measurement systems are described, covering the
frequency range 0.2 Hz to 64 MHz. The first system, for frequencies up
to 25 kHz, features a spectrum analyzer with a dual-channel fast-
Fourier transform algorithm. By exploiting the correlation feature,
the system, when combined with very low-noise preamplifiers, has a
background noise level for a low-impedance source of less than 0.3 ohms
noise resistance. The other two systems for radio frequencies use a

v

tuned step-up transformer to bring the noise of the very quiet n-type device to a level above that of the RF preamplifier. One is a conventional single-channel system. The other uses RF mixers before the dual-channel FFT analyzer to extend the range of the correlation system to high frequencies, depending on the preamplifier frequency response.

Current-voltage measurements, DC, pulsed DC, and AC impedance, are presented versus parameters bias level, temperature, and frequency, as are noise measurements. The n-type device is linear and relatively temperature independent exhibiting full thermal noise and, at low frequencies, very low levels of excess 1/f noise five orders of magnitude less than for the bulk material. This suggests that collisions are mainly absent from this device. The p-type device, conversely, is nonlinear with large levels of excess low frequency noise. There is a linear, noisy, and temperature-dependent low-bias region followed by a transition to a less noisy temperature-independent high-bias regime with large conductance. This may represent a transition from ambipolarly governed to near-ballistic transport.

CHAPTER I
INTRODUCTION

There is great interest in very thin GaAs layers of lengths
less than 1 µm. This is of the order of the mean free path lengths
of the dominant collision mechanisms for electrons. Under favorable
conditions, carriers may cross the layers undergoing few or no col-
lisions, which leads to very high velocities, much greater than the
collision-limited drift velocity. The resulting so-called ballistic or
near-ballistic transport leads to very fast-response devices for pico-
second switching at very low power or other new applications. These
new devices have been made possible by advances in fabrication tech-
niques such as electron beam lithography and, in particular, molecular
beam epitaxy.

Such small devices enable us to investigate physical mechanisms
on a small scale for which the traditional models no longer apply. In
addition, practical knowledge of the performance limitations of these
new devices is obtained.

Early theories of these devices treated the ballistic motion of
the carriers as the dominant mechanism affecting its characteristics.
Recent measurements and later theories have shown that boundary condi-
tions, in particular the velocity dispersion of the carriers, have
much greater influence.

The organization of the chapters follows. In Chapter II some
theories of small $n^+n^-n^+$ and $n^+p^-n^+$ layers in GaAs are surveyed and

1

predictions are noted. Measurement techniques and procedures are presented in Chapter III. In particular, a crosscorrelation noise measurement system with a noise resistance less than 0.3 ohms suitable for low-impedance low-noise devices such as the $n^+n^-n^+$ diode is discussed. In Chapter IV, experimental results of measurements on two devices are described. One is an $n^+n^-n^+$ structure of length 0.4 μm. The other is an $n^+p^-n^+$ device of length 0.47 μm. Current-voltage characteristics, DC, pulsed DC, and AC to 25 kHz are presented, as are measurements from 0.2 Hz to 32 MHz. The measurements are repeated at 77 K to investigate the effect of temperature. In some cases, T is reduced to 12 K. Chapter V contains a discussion of the results. Finally, conclusions and recommendations for further work are presented in Chapter VI. An HP (Hewlett Packard) 9825A computer program used to automate the noise measurements is recorded in the Appendix.

CHAPTER II
THEORY OF VERY SMALL LAYERS IN GaAs

In most semiconductor devices, the drift current is limited by the rate of carrier collisions. However, for sufficiently thin devices few or no collisions occur permitting ballistic or near-ballistic transport. The resulting carrier velocities can be much larger than in the collision-dominated case so that such parameters as switching speed can be greatly increased. Advances in fabrication techniques such as molecular beam epitaxy and electron lithography have resulted in submicron gallium arsenide devices with dimensions the same order of magnitude as the mean free paths of the dominant collision mechanisms. Thus near-ballistic transport in these devices becomes probable.

For polar optical phonon emission at room temperature, Eastman et al. [1] report mean free path lengths in GaAs of about 0.1 μm for electron energies near 0.05 eV to 0.2 μm up to 0.5 eV. Phonon absorption is about four times less probable. They also report that the change in the direction of motion due to a collision is small (5-10 degrees). Intervalley scattering becomes significant for higher electron energies than 0.5 eV. Shur and Eastman [2] calculated the mean free path in the high-purity GaAs at 77 K to be 1.3 μm. Barker, Ferry, and Grubin [3] have suggested some complicating factors even for devices of length equal to the mean free path. First, in large area

3

devices, some carriers may move at angles to the length direction, thereby increasing the distance traveled and the number of collisions. Also, some of these carriers may collide with the device boundaries. Third, space-charge effects may limit the current due to Coulomb scattering. Finally, short devices may be dominated by contact effects such as carrier reflection.

The theory for pure ballistic transport was revived from the days of vacuum tubes by Shur and Eastman [2] based on a simple model. They assumed a one-dimensional n-type device of length, L, neglecting diffusion and electron scattering. Then the current density is

$$J = qnv \tag{2.1}$$

where q is the electronic charge, n is the free electron density, and the velocity, v, is found from

$$qV_x = \frac{1}{2} m^* v^2 \tag{2.2}$$

where V_x is the voltage at x due to the applied potential, V, and m^* is the effective mass. The initial velocity and the field at the injecting contact are assumed to be zero. Poisson's equation

$$\frac{dV_x^2}{dx^2} = - \frac{q}{\varepsilon_0 \varepsilon_r} (n_0 - n) \tag{2.3}$$

is then solved yielding Child's law

$$J = \frac{4}{9} \sqrt{\frac{2q}{m^*}} \; \frac{\varepsilon_0 \varepsilon_r}{L^2} V^{3/2} \tag{2.4}$$

for large bias voltage and large consequent injected space charge. For small applied voltages, the fixed charge due to ionized donors is greater than that due to the injected carriers and an electron beam drift region ($J \sim V^{1/2}$) results. The range of voltages for which their model is valid is

$$\frac{kT}{q} < V < \frac{\Delta E}{q} \tag{2.5}$$

where T is the lattice temperature and ΔE is the energy difference between the main conduction band minimum and the secondary valley. For very small voltages diffusion cannot be neglected. Intervalley scattering is the cause of the upper voltage limit. Some measurements [1,4] have been reported that appear to support this model, but their interpretation has been questioned as will be discussed.

To take into account the effect of a few collisions, Shur [5] and Shur and Eastman [6] have extended the theory. Frictional "drag terms" to represent the collisions are added to the equations of balance of energy and momentum. In general, the effective mass, m^*, and relaxation times, τ_m and τ_E, are functions of energy so that the balance equations are

$$\frac{dm^*(E)v}{dt} = qE - \frac{m^*(E)v}{\tau_m(E)} \tag{2.6}$$

and

$$\frac{dE}{dt} = qEv - \frac{E - E_0}{\tau_E(E)}$$ (2.7)

Shur assumes a constant energy-independent effective mass and a single momentum relaxation time, τ, so that, neglecting (2.7), (2.6) is replaced by

$$m^\star \frac{dv}{dt} = qE - \frac{m^\star v}{\tau}$$ (2.8)

Equations (2.1), (2.3), and (2.8) along with the boundary conditions for the ballistic case are then solved analytically. For τ much longer than the transit time and sufficient applied voltage to justify neglecting n_0, Child's law is again obtained. Conversely τ much less than the transit time yields (for $V = -\mu E$ where μ is the mobility) the Mott-Gurney law for collision-dominated space-charge limited current

$$J = \frac{9}{8} \varepsilon_0 \varepsilon_r \mu \frac{V^2}{L^3}$$ (2.9)

In the second paper, values of $m^\star(E)$, $v(E)$, $\tau_m(E)$, and $\tau_E(E)$ are obtained from Monte Carlo calculations. Steady state is assumed and the boundary conditions are taken to be the initial field (and velocity) equal to zero. Again letting τ_E and τ_m become large yields Child's law. For the general case, computer solutions are presented for various lengths and doping densities which show small deviations from their previous (ballistic) results.

The interpretation that current proportional to $V^{3/2}$ indicates ballistic transport has been seriously questioned by some authors. Rosenberg, Yoffa, and Nathan [7] have shown the crucial importance of the boundary conditions. For the ballistic case, they assumed a simple one-dimensional model neglecting collisions. For each electron, they solve equations (2.1), (2.3), and the energy-velocity relationship

$$\frac{m^*}{2} (v^2 - v_i^2) = q(V_i - V) \tag{2.10}$$

where v_i and V_i are the initial velocity and potential, respectively. A displaced Maxwellian distribution of initial velocities characterized by a temperature and mean velocity is assumed. A set of nonlinear equations in V result which are solved numerically for specified electric field, E, initial carrier density, n_i, and initial (temperature normalized) mean velocity, $\bar{v}$. They demonstrate that a wide variety of current versus potential curves can be generated for various choices of initial conditions [7, Figure 3]. The authors agree with others [3,8] that, conversely with Shur and Eastman, the current-voltage characteristic may be used to infer the boundary conditions for a device that has already been shown to be ballistic by other means (such as noise behavior).

Another significant effect in short devices is "spillover" of carriers from high- to low-doped regions. The result is that the effective length of the low-doped region is shortened and hence the resistance is less than expected naively even for devices many Debye lengths long [7]. Universal curves have been calculated by van der Ziel

et al. [9] from which the magnitude of the effect can be determined for a particular device. The authors calculated the near-equilibrium resistance for a 0.4 μm n-type device with doping densities N_{d+} = 10^{18} cm^{-3} and N_{d-} = 10^{15} cm^{-3} for liquid nitrogen and room temperatures. They solve Poisson's equation including electrons and ionized donors in the high- and low-doped regions, neglecting holes. They assume

$$n(x) = N_{d+} \exp\left(\frac{q\psi(x)}{kT}\right) \tag{2.11}$$

where N_{d+} is the ionized donor density in the highly doped region and $\psi(x)$ is the potential. Reciprocal mobilities due to diffusion/drift and thermionic emission are added to give an effective mobility which agrees within 10% of experimental results at room temperature. However, a similar calculation for an $n^+p^-n^+$ device is off by more than an order of magnitude. They assumed that the electron spillover depletes the holes in the p-region such that they (holes) may be neglected. This is apparently not the case; the effects of the holes are important.

The simple theory of ballistic [2] and near-ballistic [5,6] transport does not take into account the energy or velocity distributions of the carriers. Cook and Frey [10] have suggested the inclusion of an electron temperature gradient term in the momentum balance equation for this purpose. This may be sufficient for first order effects such as the current-voltage characteristic. Their treatment includes an average collective velocity dispersion term, in essence treating the ensemble as a single particle for such effects as the

noise, a drawback they themselves point out in the simple theory. For the noise, more adequate analysis should include a Langevin or Monte Carlo approach based on the momentum and energy balance equations which include terms necessary to account for the significant physical mechanisms. Such a Monte Carlo calculation for a 0.25 μm n^+-i-n^+ diode at 77 K has been reported by Awano et al. [11]. Ionized impurity and intervalley and intravalley phonon scattering is included in their model but not nonparabolicity of the band edges. Particles with a distribution of velocities in equilibrium with the lattice at 77 K are injected at one contact. They find that a large proportion of the particles are transported ballistically. Groups of particles corresponding to one or two collisions and some backscattering from the collecting contact is observed. For potentials less than 0.5 volts, the current-voltage characteristic is surprisingly close to Child's vacuum diode law.

Holden and Debney [12] have presented a calculation based on ideas from Fry's theory for thermionic values [13]. They assume injection from both n^+ regions of carriers with Maxwell-Boltzmann velocity distributions. Scattering is neglected. Following Fry, the free-carrier charge density is found by an integration over the injected carrier velocity distribution. A potential minimum due to injected space-charge is assumed. They calculate current-voltage characteristics for T = 77 K and lengths of 0.1, 0.2, and 0.5 μm. The slopes at high bias are less than 3/2 (L = 0.1 and 0.2 μm give $\sim$1.3, L = 0.5 μm gives $\sim$1.14). At low bias, the characteristics are somewhat more linear.

The authors conclude that ballistic effects do not lead to a particular current-voltage power law and suggest that another method must be found to determine ballistic effects.

The noise behavior of thin structures gives important information on the extent of ballistic effects. Current-voltage characteristics for these devices are dominated by events at the boundaries such as the carrier velocity distribution. In addition, practical knowledge of the performance limitations of the devices is obtained, as well as useful insight into the physical mechanisms causing the various types of noise.

The noise is naturally divided into two frequency regions. At high frequencies the dominant mechanism, variously called thermal, velocity fluctuation, or diffusion noise is the electrical result of the Brownian motion of the carriers. While the theory is not yet complete, preliminary calculations have been made by van der Ziel and Bosman [14,15]. For the ballistic case (collisions neglected) at large bias, the device is modeled similarly to a dual-cathode vacuum diode with opposing thermionic emission currents across the potential minimum. Then correlated fluctuations in the current due to fluctuations in the minimum due to the space charge result in a lowered (64%) level of noise compared to the low-bias value of thermal noise of the AC conductance. For the collision-limited case, at sufficiently large bias, the device is modeled as a space-charge-limited solid-state diode and the noise becomes twice the thermal noise of the AC conductance. Thus ballistic effects should reduce the noise and

collision-dominated transport should increase it if sufficient bias levels can be achieved.

At low frequencies, excess noise characterized by a spectral density with a 1/f frequency dependence dominates. According to most recent theories [16,17] such noise is thought to be caused by mobility fluctuations which represent fluctuations in scattering cross-sections. The usual method to describe the noise is using Hooge's empirical formula [18]

$$S_{\Delta I}(f) = \frac{\alpha_H I_0^2}{fN} \tag{2.12}$$

where I_0 is the dc current, N is the number of carriers, f is the frequency, and α_H is Hooge's parameter.

This is accurate for a uniform sample. However, for a non-homogeneous sample or a mesa structure, van der Ziel and Van Vliet [19] have shown that the formula becomes

$$S_{\Delta I}(f) = \frac{m\alpha_H I_0^2}{fAL^2} \int_0^L \frac{dx}{n(x)} \tag{2.13}$$

where m is the number of layers, L is the length of one layer, A is the cross-sectional area, and n(x) is the electron density. The value of α_H was first thought to be constant (2×10^{-3}). Later research has found that α_H depends on material variation, the dominant scattering mechanism, and carrier heating [20] in Si. Thus the magnitude of α_H should give a good measure of the rate of collisions or lack of them.

The procedures used in the measurement of both devices, $n^+n^-n^+$ and $n^+p^-n^+$, are similar, but the actual circuits depend on the device characteristics which are quite different. The p-type near-ballistic diode (NBD) exhibited an impedance about 100 times that of the n-type device at small bias. It also generated excess noise at low frequencies orders of magnitude larger than the n-type NBD. Consequently, the noise of the n-NBD was the most challenging measurement requiring an equivalent noise resistance of the measurement system of about 0.2 ohms.

3.1 Current Voltage Measurements

Three I-V measurements were done on each diode: DC, pulsed DC, and AC from 2.4 Hz to 25 kHz. A block diagram of the n-NBD circuit is shown in Figure 3.1. A three-terminal measurement is required since the resistance of the active region is comparable to that of the bonding wire to the top surface of the diode (the devices were mounted in TO-5 cans). The resistance of the output wire, R_{L2}, is negligible since it is in series with the large input impedance of the oscilloscope. Then V_2 is the voltage across $R_X + R_S$ which represents the series combination of substrate resistance and active region. The current through the device is

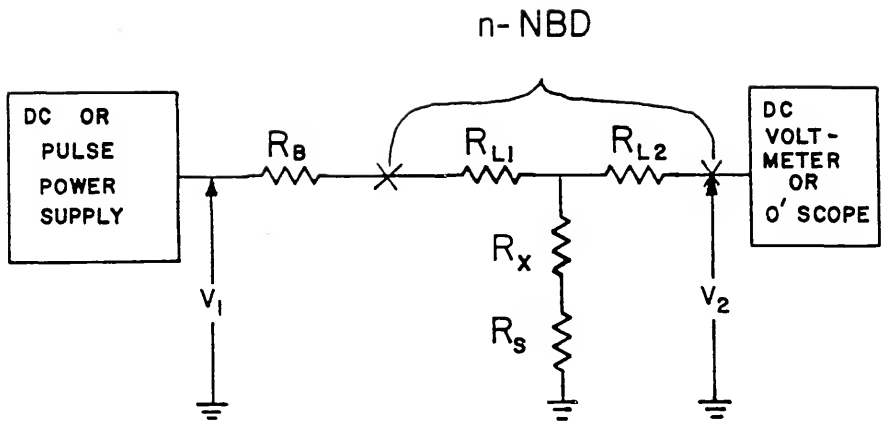$$I = \frac{V_1 - V_2}{R_B + R_{L1}}$$

(3.1)

12

Figure 3.1 Block diagram of $n^+n^-n^+$ diode current-voltage measurement

Pulsed measurements were done using an HP 214A pulse generator. The pulse width was 1 μsec and the repetition rate was 100 Hz.

The AC I-V measurement employed the HP 3582A spectrum analyzer. The dual-channel feature was used to measure the transfer function as a function of frequency from 2 Hz to 25 kHz and as a function of DC bias. The circuit diagram of the AC resistance measurement is shown in Figure 3.2. Taking into account the parallel resistances, R_X is found to be

$$R_X = \frac{\frac{V_0}{V_C}\left[R_C\left(1 + \frac{R_S + R_{L1}}{R_B}\right) + R_S + R_{L1}\right] - R_S}{1 - \frac{V_0}{V_C}\left(1 + \frac{R_C}{R_B}\right)} \qquad (3.2)$$

The measurement for the p-type device is similar. Here, the lead resistances may be neglected since the impedance is large; the diode may be treated as a two-terminal device.

3.2 The 0.24 Hz to 25 kHz Correlation System

For the electrical noise measurement of low impedance devices with resistances of the order of an ohm, the usual single-channel method is not useful. Typical preamplifiers have noise resistances of about 10 to 20 ohms. The device noise is masked by the preamplifier noise. Therefore, the correlation method [21] is used as shown in Figure 3.3.

A Hewlett Packard 3582A spectrum analyzer featuring a dual-channel Fast-Fourier transform is employed. Low-noise preamplifiers
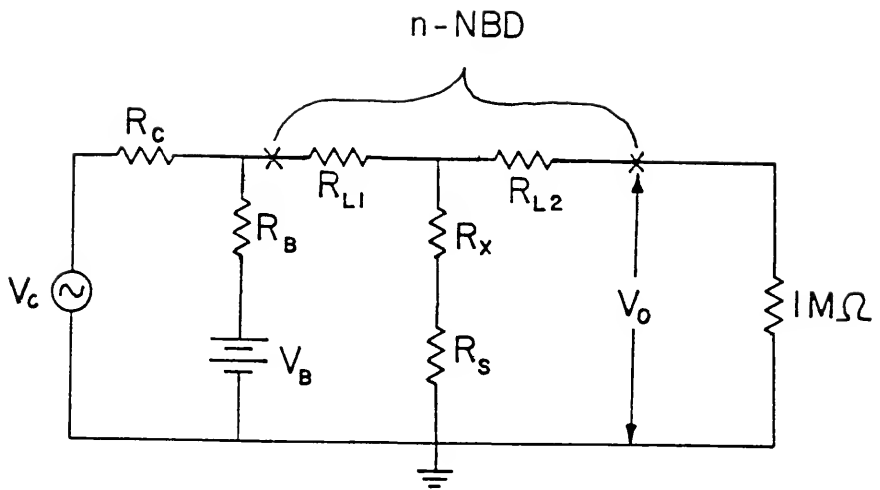
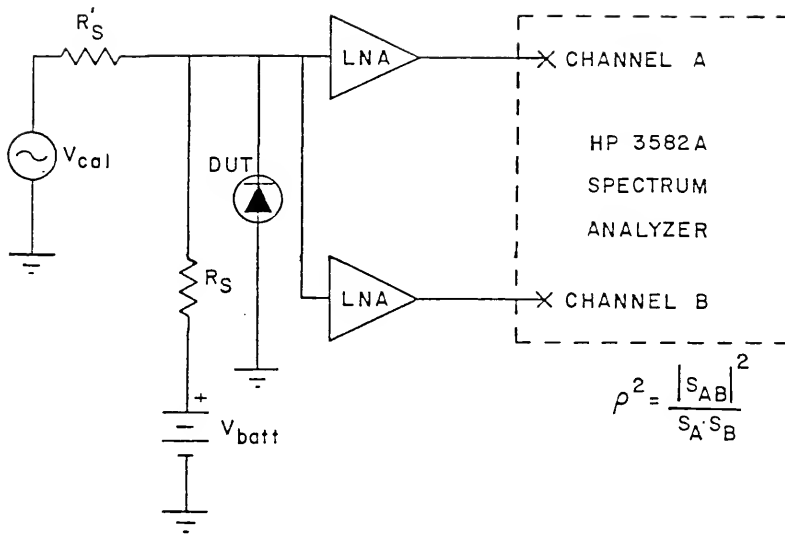Figure 3.2 AC resistance measurement circuit for n-NBD

Figure 3.3 Correlation measurement setup

precede each channel from a common input. By measuring the coherence (square of the correlation between the channels) the cross-spectra can be calculated. The noise generated at the output of each channel is uncorrelated with the other and therfore averages out in the final reading. Only the noise generated at the input of each channel gives a contribution to the final reading. Hence a better device noise versus amplifier background noise ratio may be obtained.

The device under test (DUT) noise is compared to a known calibration signal which is applied through a series resistor much greater than the DUT resistance. The bias current is applied in a similar manner. An equivalent circuit of the measurement setup is shown in Figure 3.4. To characterize the noise of the system, we first neglect the effect of the device noise. The series resistors to the bias and calibration sources are R_S' and R_S. The calibration source, v_{cal}, transforms to a Norton equivalent, i_c, where

$$i_c = \frac{v_{cal}}{R_S'} \tag{3.3}$$

The source resistance is represented by R_X. The preamplifiers are assumed identical (with uncorrelated noise sources, v_1, i_1, v_2, and i_2) with gain, G (assumed constant), and input resistance, R_i. The output of the amplifiers, u_1 and u_2, are then multiplied together and averaged.

The measurement procedure is to compare the output for three conditions. They are (1) shorted input ($R_X = 0$) giving output reading M_1, (2) open input ($R_X = \infty$, $R_S \parallel R_S' \gg R_i$) giving M_2, and (3) open input
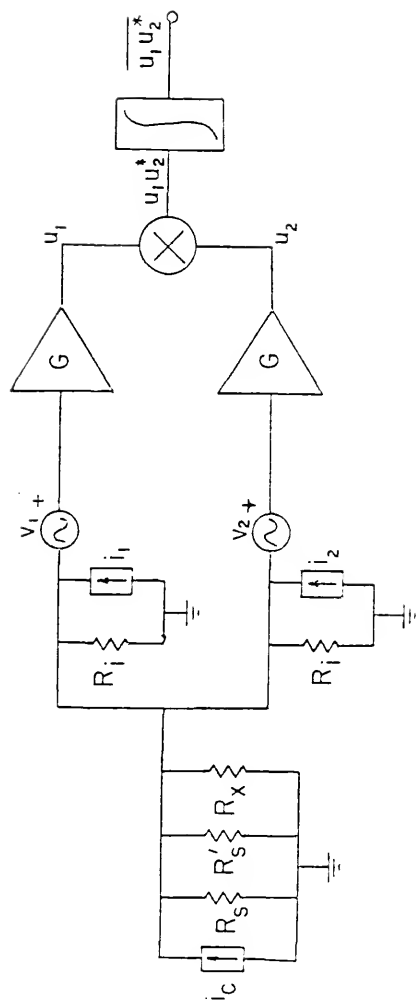
Figure 3.4 Measurement setup equivalent circuit

with calibration signal applied ($i_c \neq 0$) which gives M_3. The output for each case is easily found to be

$$M_1 = 0 \tag{3.4}$$

$$M_2 = G^2 \, (\overline{i_1 i_1^\star} + \overline{i_2 i_2^\star}) \, \frac{R_i^2}{4} \tag{3.5}$$

and

$$M_3 = G^2 \, (\overline{i_1 i_1^\star} + \overline{i_2 i_2^\star} + \overline{i_c i_c^\star}) \, \frac{R_i^2}{4} \tag{3.6}$$

In reality, M_1 is not exactly zero. There is a residual background noise. This can be accounted for by introducing a correlated background noise source, v_b, to the input voltage sources so that $v_1 = v_1' + v_b$ and $v_2 = v_2' + v_b$. The primed portions are uncorrelated. Then the analysis yields

$$M_1 = G^2 \, \overline{v_b v_b^\star} \tag{3.7}$$

$$M_2 = G^2 \left[\overline{v_b v_b^\star} + (\overline{i_1 i_1^\star} + \overline{i_2 i_2^\star}) \, \frac{R_i^2}{4} \right] \tag{3.8}$$

and

$$M_3 = G^2 \left[\overline{v_b v_b^\star} + (\overline{i_1 i_1^\star} + \overline{i_2 i_2^\star} + \overline{i_c i_c^\star}) \, \frac{R_i^2}{4} \right] \tag{3.9}$$

Writing the mean square averages as spectral densities, i.e.,
$S_{Ic} = 2 \frac{\overline{i_c i_c^*}}{\Delta f}$, etc., and noting $S_{Ic} = \frac{S_{Vc}}{R'^2_S}$, allows the current and
voltage noise to be calculated.

$$K = \frac{M_3 - M_2}{M_2 - M_1} = \frac{S_{Ic}}{S_{I1} + S_{I2}} \tag{3.10}$$

Thus

$$S_{I1} + S_{I2} = \frac{S_{Vc}}{K R'^2_S} \tag{3.11}$$

and

$$S_{Vb} = \frac{R_i^2 S_{Vc}}{K R'^2_S \left(\frac{M_2}{M_1} - 1 \right)} \tag{3.12}$$

The current noise spectra of the two channels are S_{I1} and S_{I2} and the
background voltage noise spectrum is S_{Vb}.

A significant source of background noise, after such causes
as pickup of unwanted signal, ground loops, and power supply noise have
been eliminated, is the finite averaging time of the spectrum analyzer.
The sample coherence for shorted input versus number of averages is
shown in Figure 3.5. It is a large-side biased estimate inversely pro-
portional to the number of averages which is limited to 256. The
distribution of sample coherences is not easily described [22] for
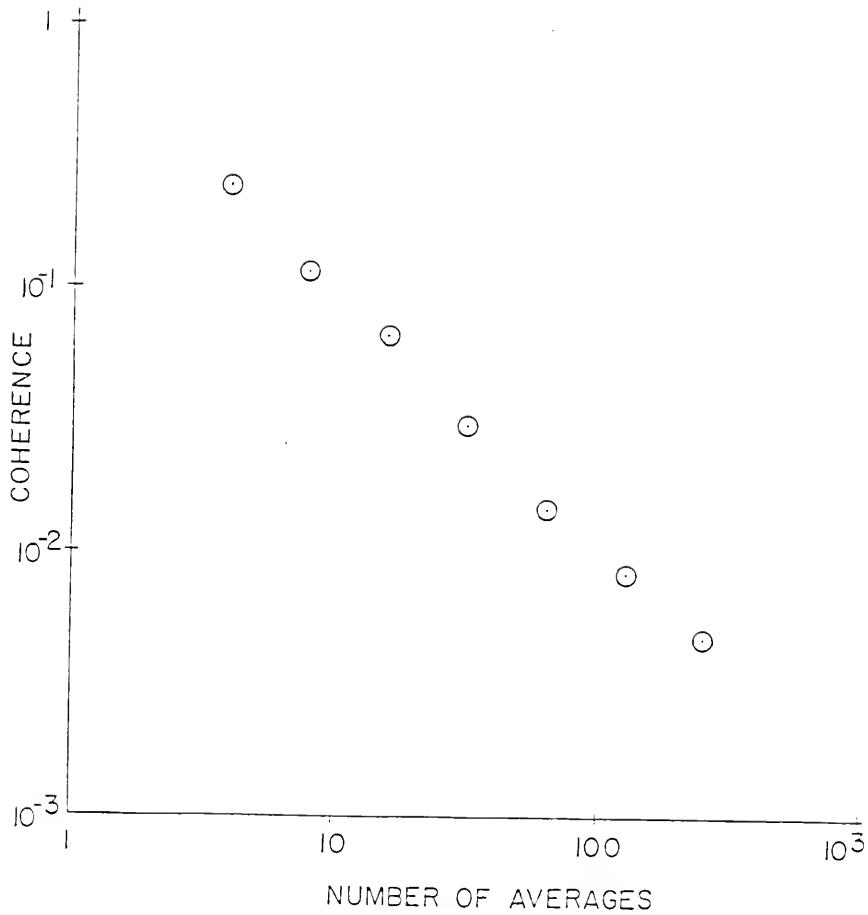
Figure 3.5 HP 3582A sample coherence for shorted input versus number
           of averages

small expected value. The residual nonzero value is interpreted as background noise.

The system is used with two similar sets of preamplifiers denoted PA1 and PA2; PA2 features five parallel input stages like that of PA1 but with larger bias current. They are shown in Figures 3.6 and 3.7; PA1 has larger voltage noise but extended low frequency response suitable for excess 1/f noise measurement. The PA2 has been designed for minimum voltage noise.

The PA1 features a capacitively coupled common emitter transistor first stage with shunt feedback. This reduces the input impedance but does not affect the noise. The primary motivation for this circuit is a practical one. The RC settling time of the base bias circuit is substantially reduced compared to the usual configuration. The transistor (GE 82) is chosen for large β and small series base resistance. The second stage is a low-noise operational amplifier (Burr-Brown OPA101BM) in noninverting configuration; 12-volt automotive batteries are used for the power supply.

An equivalent circuit of the input stage is shown in Figure 3.8. It is the low-frequency hybrid pi including source resistance, feedback, and noise sources. The source resistance is R_S. Thermal noise of the series base resistance, r_b, is v_b. Shot noise of the base and collector currents are denoted i_b and i_c, respectively. To transform this circuit to a form similar to that in Figure 3.4, the closed loop gain, the input resistance, and the noise sources must be calculated. The closed loop gain is found by summing currents at
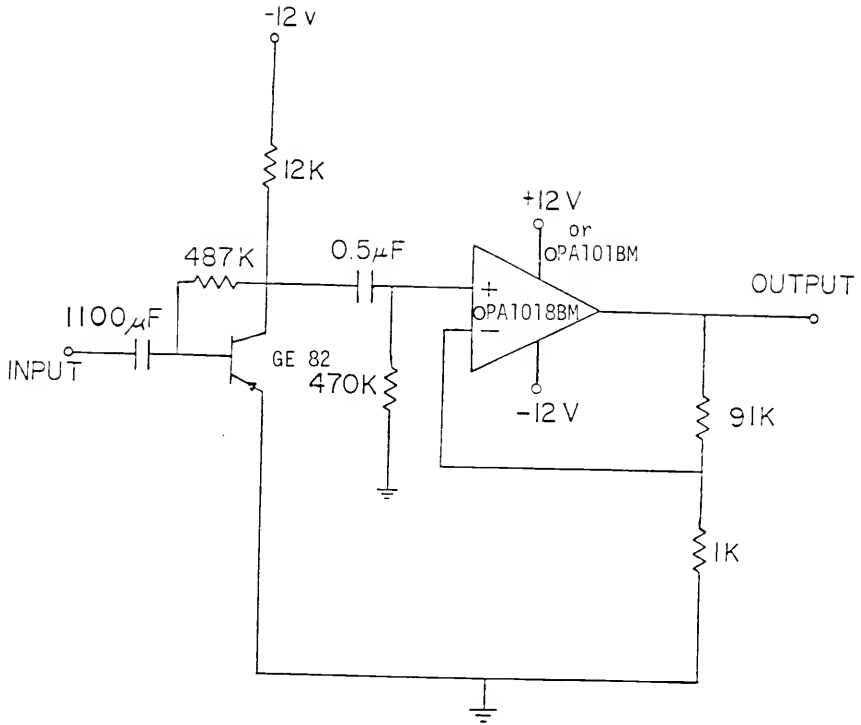
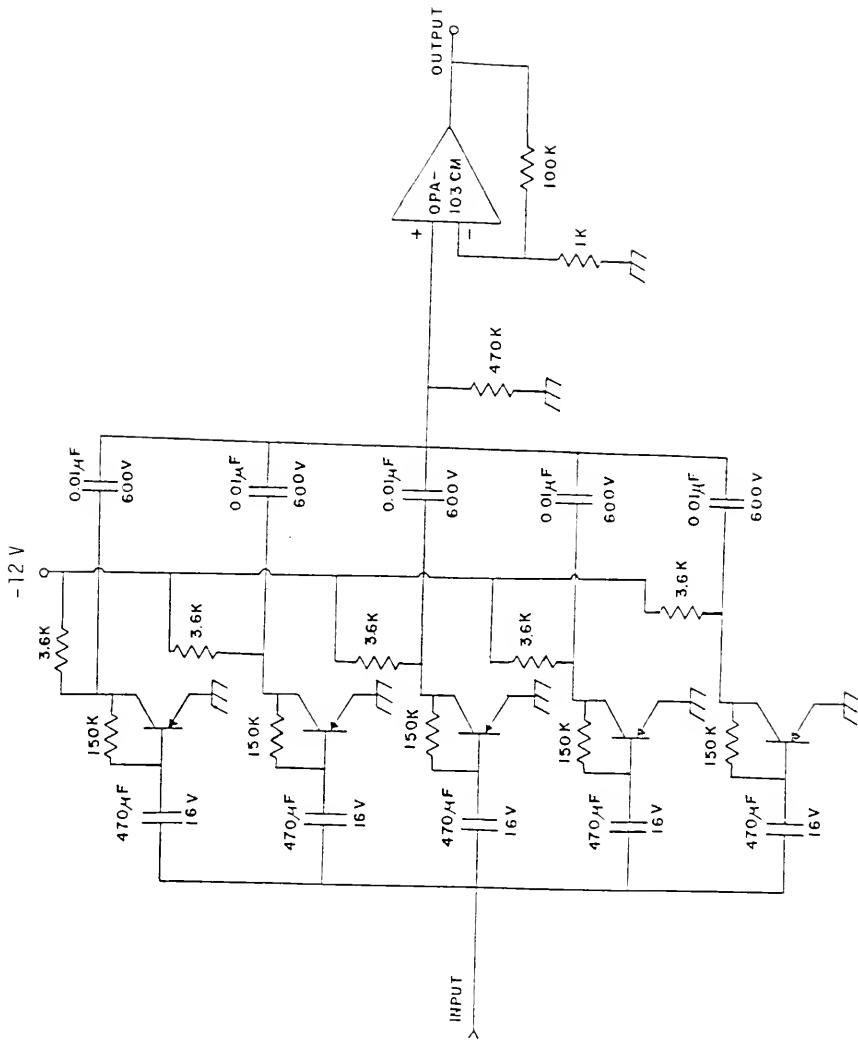Figure 3.6. Model one (PA1) low-noise premplifier
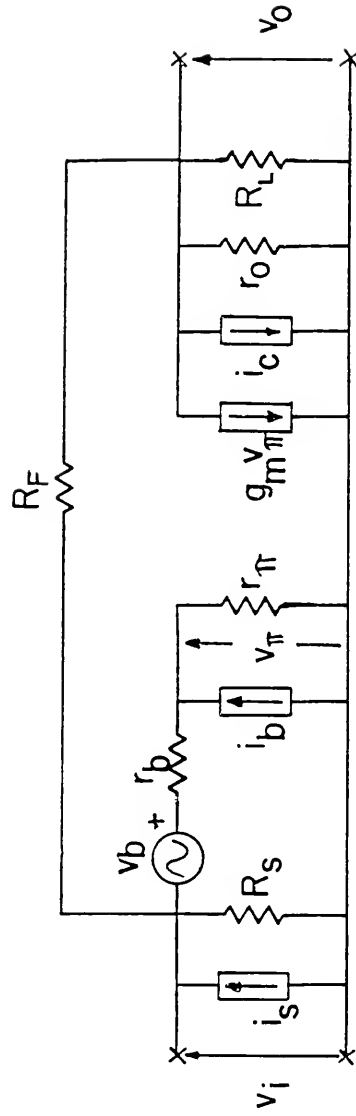
Figure 3.7 Model two (PA2) low-noise preamplifier

Figure 3.8 PA1 input stage equivalent circuit

the input

$$i_s + \frac{v_o - v_i}{R_F} - i_i - \frac{v_i}{R_S} = 0,$$ (3.13)

and at the output

$$\beta i_i + \frac{v_o - v_i}{R_F} + \frac{v_o}{R_C} = 0$$ (3.14)

where $R_C = r_o \parallel R_L$, $\beta i_i = g_m v_\pi$ and the noise sources have been neglected for now. Letting $r_i = r_b + r_\pi$ so $i_i = \frac{v_i}{r_i}$, the output equation gives i_i in terms of v_o which, when substituted into the input equation allows i_s to be expressed as a function of v_o. Then, for $R_F \gg \frac{r_i}{\beta}$, the closed loop gain, A, is found to be

$$A = \frac{v_o}{i_s} \simeq \frac{-R_F}{1 + \frac{R_F + R_C + r_i \left(1 + \frac{R_C}{R_F}\right)\left(1 + \frac{R_F}{R_S}\right)}{\beta R_C}}$$ (3.15)

The loop transmission is found by disconnecting the output current generator, $g_m v_\pi$, and applying a test current generator, i_T, there. The output voltage, v_o, is

$$v_o = i_T [R_C \parallel (R_F + R_S \parallel r_i)]$$ (3.16)

The input voltage fed back is

$$v_i = \frac{r_i R_S}{r_i + R_S} \frac{(v_o - v_i)}{R_F} \tag{3.17}$$

so that

$$v_i = v_o \frac{\dfrac{r_i R_S}{(r_i + R_S) R_F}}{1 + \dfrac{r_i R_S}{(r_i + R_S) R_F}} \tag{3.18}$$

Then, noting that $g_m v_\pi = g_1 v_i$ gives

$$T = \frac{g_m v_\pi}{i_T} = \frac{-\beta R_C}{\left(R_C + R_F + \dfrac{R_S r_i}{R_S + r_i}\right)\left(1 + \dfrac{r_i}{R_S}\right)} \tag{3.19}$$

The input resistance is R_S in parallel with R_i where, for $R_F \gg R_C$ and $R_F \gg r_i/\beta$,

$$R_i \simeq r_i \parallel \frac{R_C + R_F}{1 + \dfrac{r_\pi}{r_i} R_C g_m} \tag{3.20}$$

The output resistance is R_o in parallel with R_L where

$$R_o = r_o \parallel \frac{R_F + r_i + \dfrac{r_i R_F}{R_S}}{\beta + 1 + \dfrac{r_i}{R_S}} \tag{3.21}$$

Except for the noise, the circuit of Figure 3.8 now becomes that of
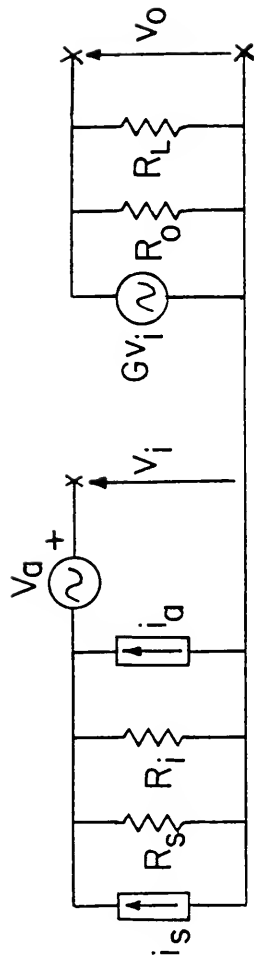Figure 3.9 where the voltage gain is

Figure 3.9 Transformed equivalent input circut of PA1

$$G = A \left(\frac{R_S + R_i}{R_S R_i} \right) \tag{3.22}$$

For the case that $R_F \gg R_C$, r_i, $R_i \gg r_b$, R_S, and $(r_i R_F)/R_S \gg \beta R_C$, then

$$G \simeq \frac{-\beta R_C}{r_i} \tag{3.23}$$

The gain becomes open loop as the input is shorted by a small R_S. To transform the noise sources, the effect of feedback is neglected. Open circuiting the inputs ($R_S = \infty$) of Figures 3.8 and 3.9 and setting the output voltages equal yields

$$i_a = i_b \left(1 + \frac{r_b}{r_b + r_\pi} \right) - \frac{v_b + \dfrac{i_c}{g_m}}{r_b + r_\pi} \tag{3.24}$$

Short circuiting ($R_S = 0$) the inputs yields

$$v_a = v_b + \frac{i_c}{g_m} + i_b r_b \tag{3.25}$$

Substituting numerical values for components with $R_S = 5.6$ ohms and assuming $\beta \sim 350$ yields about 1200 ohms for the input resistance. The measured value for two PA1s in parallel is 660 ohms as shown in Figure 3.10. The input resistance of two PA2s in parallel is shown in Figure 3.10. For the gain the calculated value is about 51 decibels. The result including the second stage is 90 decibels. The measured value is 89.5 decibels as shown in Figure 3.12.
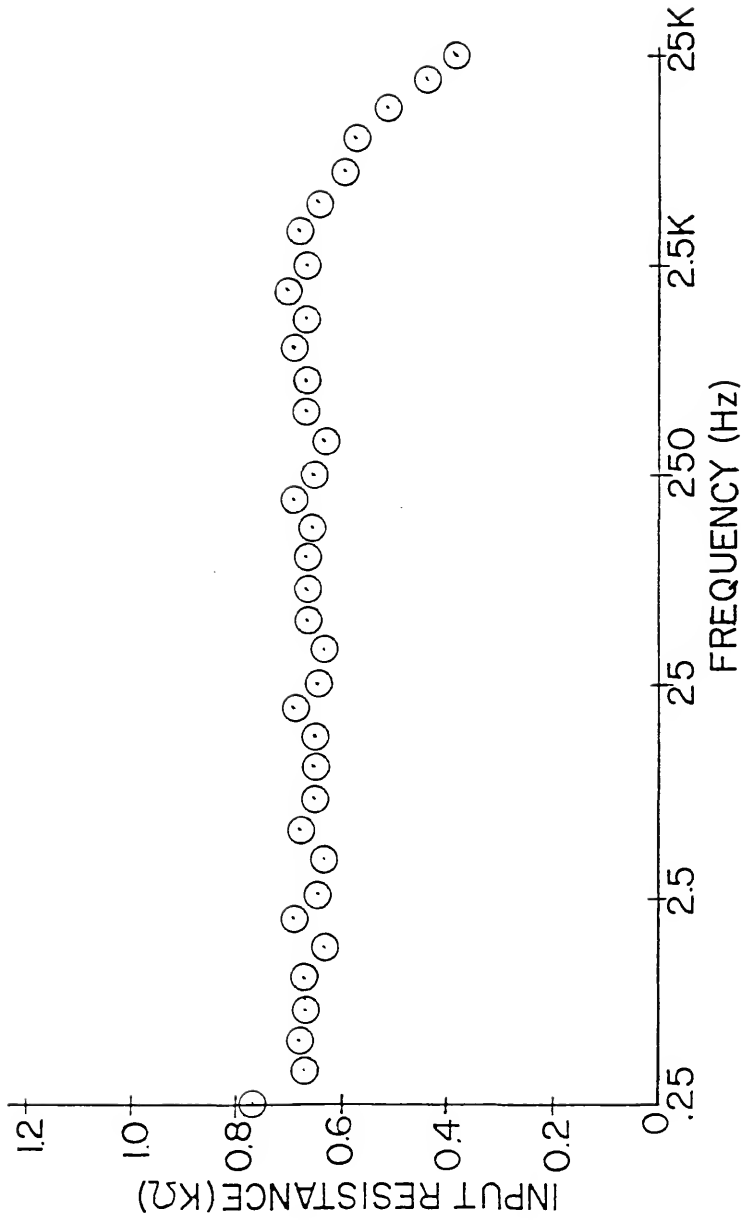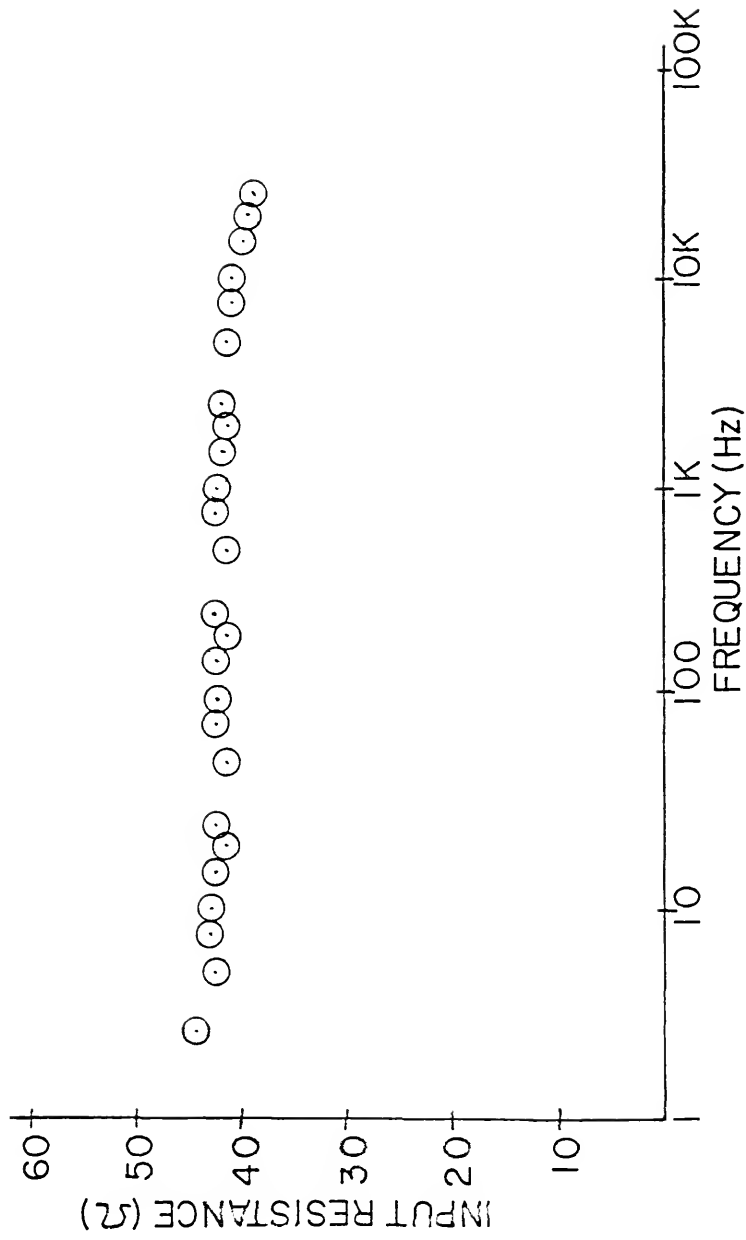
Figure 3.10 PA1 input resistance

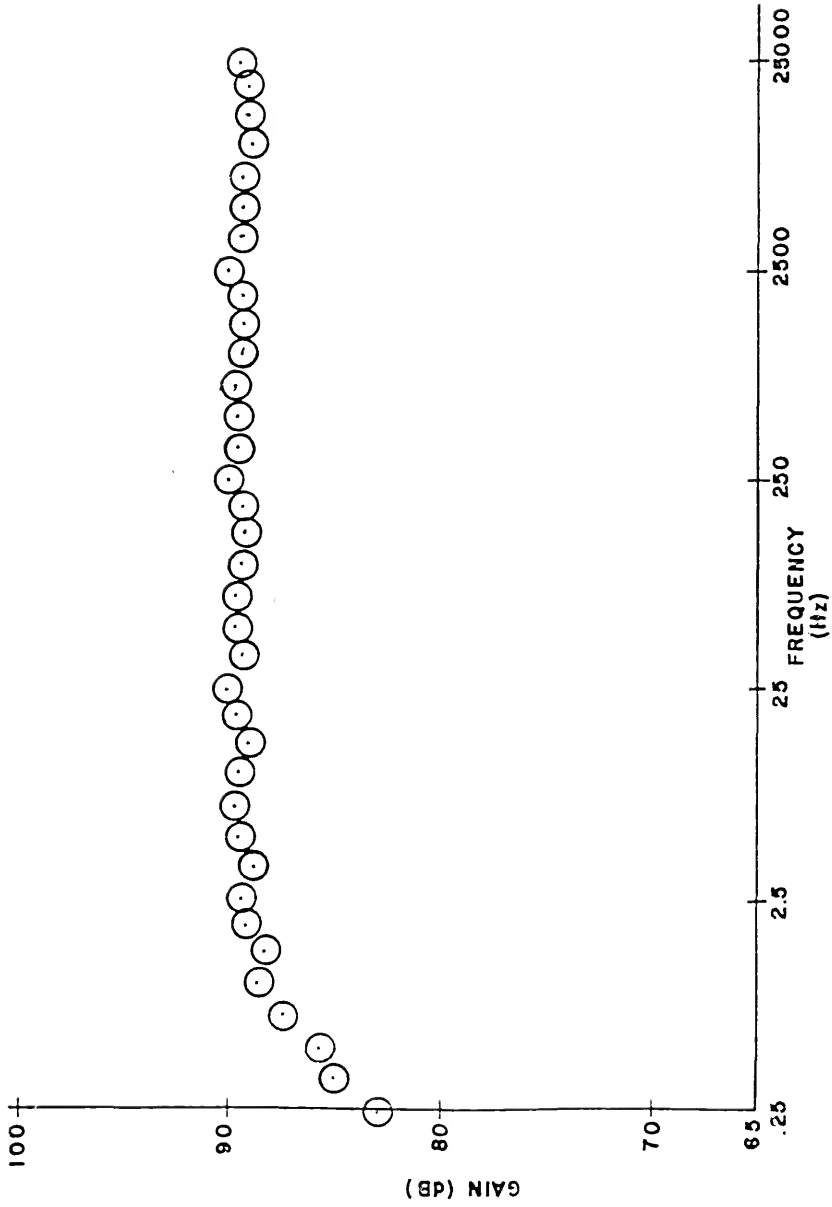Figure 3.11   PA2 system input resistance

Figure 3.12 PA1 single-channel gain

The noise resistance of PA1 and PA2 were measured to be about 35 and ⌐2.5 ohms, respectively. The five in parallel input stage of the PA2 gives that factor of reduction in the noise resistance. Another factor of three reduction comes from increasing the input bias currents by that amount since, to first order approximations, the voltage noise sources are inversely proportional to bias [23].

Using the correlation setup gives about a factor of ten reduction in the voltage noise. This is seen in the plots of voltage noise resistance and current noise conductance for the two setups shown in Figures 3.13 through 3.16. The noise resistance, R_n, is defined by

$$S_{Vb} = 4kTR_n \tag{3.26}$$

Similarly, the noise conductance is defined by

$$S_{I1} + S_{I2} = 4kTG_n \tag{3.27}$$

The current noise of the PA2 is much larger than that of the PA1 as would be expected from larger bias currents and five in parallel. For the sensitive measurements, the current noise is shorted by the small resistance of the DUT. This is the full current noise which remains in the correlation calculation. Of the voltage noise, only the background level remains.

The device noise measurement procedure is very similar to that for the amplifier. Three conditions are recorded. They are (1) DUT on, (2) DUT off, and (3) calibration signal applied with DUT off. Any change in DUT resistance between the on and off state must be

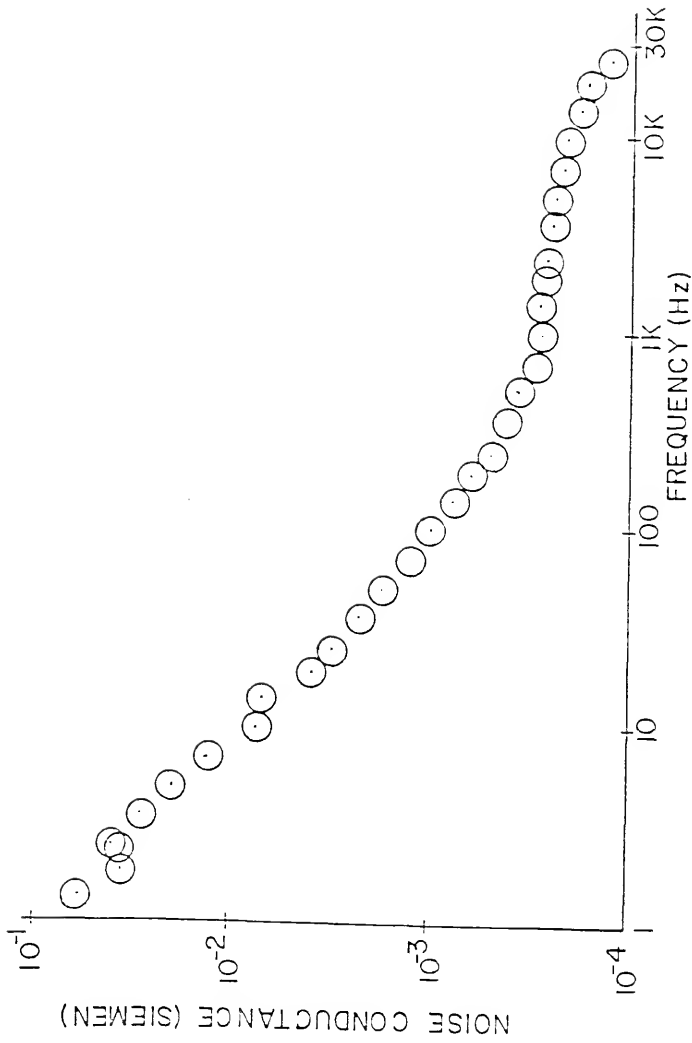Figure 3.13 Correlation system voltage noise with PA1

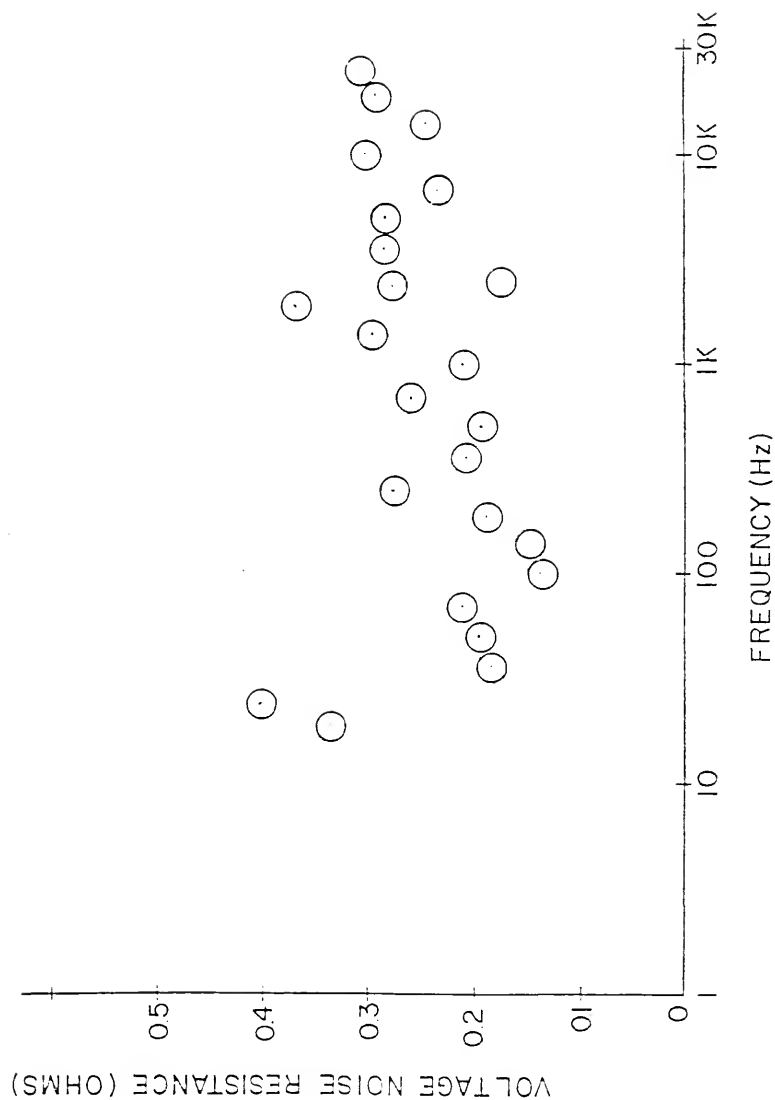Figure 3.14 Correlation system current noise with PA1
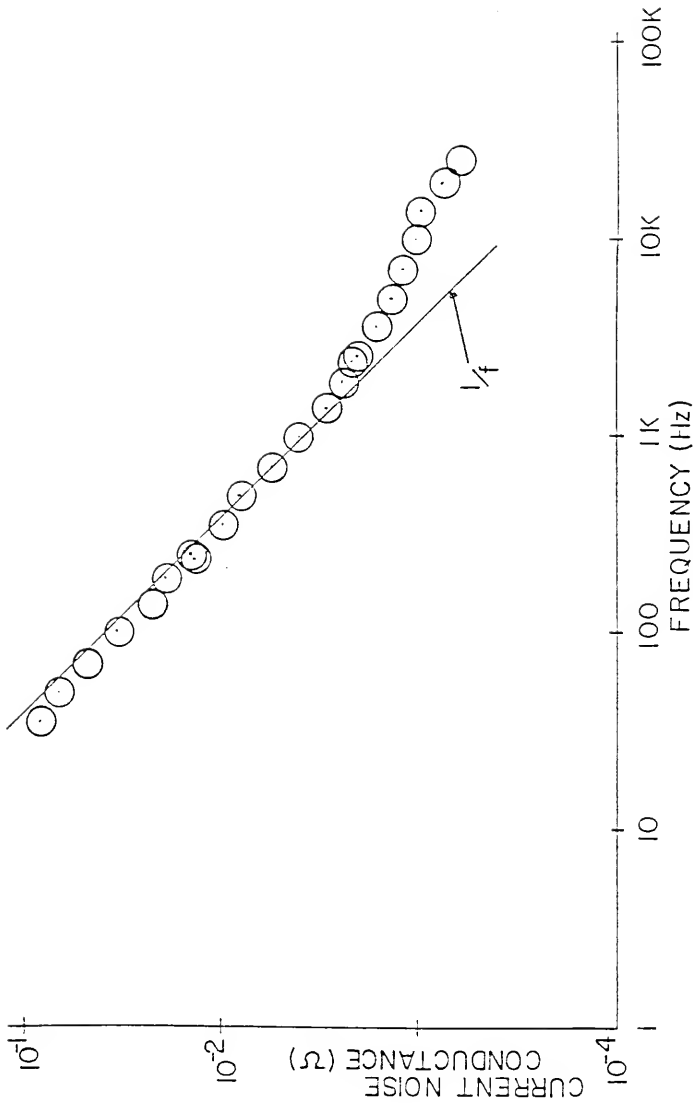
Figure 3.15   Correlation system voltage noise with PA2

Figure 3.16 Correlation system current noise with PA2

taken into account (replacing the device by a resistance equal to its "on" resistance for the latter two measurements). The equivalent circuit of the input can be drawn as in Figure 3.17. The DUT is represented by the parallel combination of R_x, the AC resistance of the device, $\sqrt{S_{th}\Delta f}$, the thermal current noise generator, and $\sqrt{S_x\Delta f}$ the excess current noise generator. The calibration signal is $\sqrt{S_{cal}\Delta f}$. The amplifier is characterized by R_a, $\sqrt{S_A^i\Delta f}$ and $\sqrt{S_A^v\Delta f}$

For the three conditions, the outputs are

$$M_1 = G^2[(S_x + S_{th} + S_A^i)R^2 + S_A^v] \tag{3.28}$$

$$M_2 = G^2[(S_{th} + S_A^i)R^2 + S_A^v] \tag{3.29}$$

and

$$M_3 = G^2[(S_{th} + S_A^i + S_{cal})R^2 + S_A^v] \tag{3.30}$$

where G is the (constant) gain and R is the parallel resistance at the input. Then, as before,

$$K = \frac{M_1 - M_2}{M_3 - M_2} = \frac{S_x}{S_{cal}} \tag{3.31}$$

so that the device noise current can be written

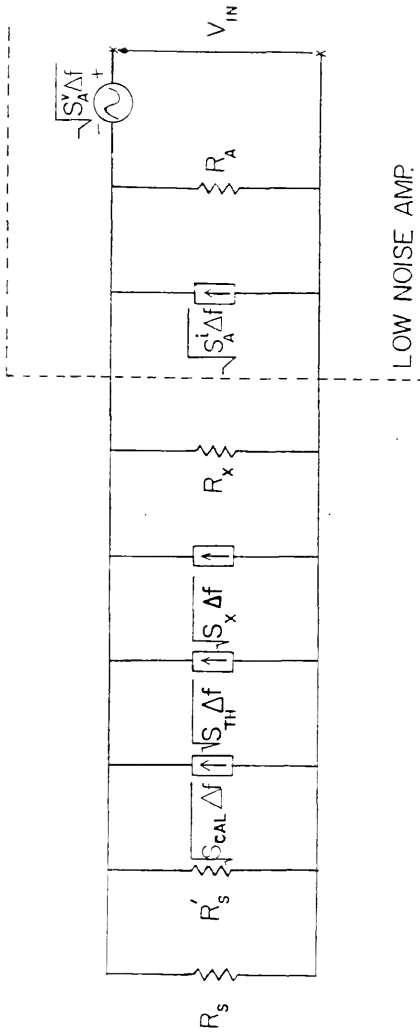$$S_{DUT} = S_x + S_{th} = K\,S_{cal} + \frac{4kT}{R_x} \tag{3.32}$$

Figure 3.17 Noise equivalent circuit of the measuring setup

Note that for the nonlinear $n^+p^-n^+$ diode, $R_x = \frac{dV}{dI}$ and depends on the bias current applied. An HP 9825A controller can easily automate this measurement and be used to average many data sets for increased accuracy. A program which does this for eight logarithmically spaced points per decade is presented in the Appendix.

3.3 The 50 kHz to 32 MHz System

At radio frequencies, the same three-measurement procedure as before is used for the noise. The circuit is more conventional, as shown in Figure 3.8. A step-up transformer consisting of four transmission line transformers in cascade with capacitance-tuned input and output is employed for the n-type device. See the Radio Amateur's Handbook for details. A Micronetics KSD2OLEE solid-state noise source is used for the calibration signal. Frequency selection is done by an HP 8557A spectrum analyzer. The IF output signal from the spectrum analyzer is passed through a 21 MHz bandpass filter and detected with an HP 431C power meter.

The preamplifier, designed and built by Christopher Whiteside of the noise research group, is shown in Figure 3.19. It employs two stages of low-noise FETs (2N4393) in cascade configuration to obtain 30 dB gain with a noise voltage resistance of about 70 ohms. This is less than the stepped-up noise of the DUT.

The HP 3582A spectrum analyzer can be used to make noise measurements in the radio frequency range. This is accomplished by mixing down the RF signal just before the analyzer as shown in Figure 3.20. Only a single channel is shown, although the correlation method
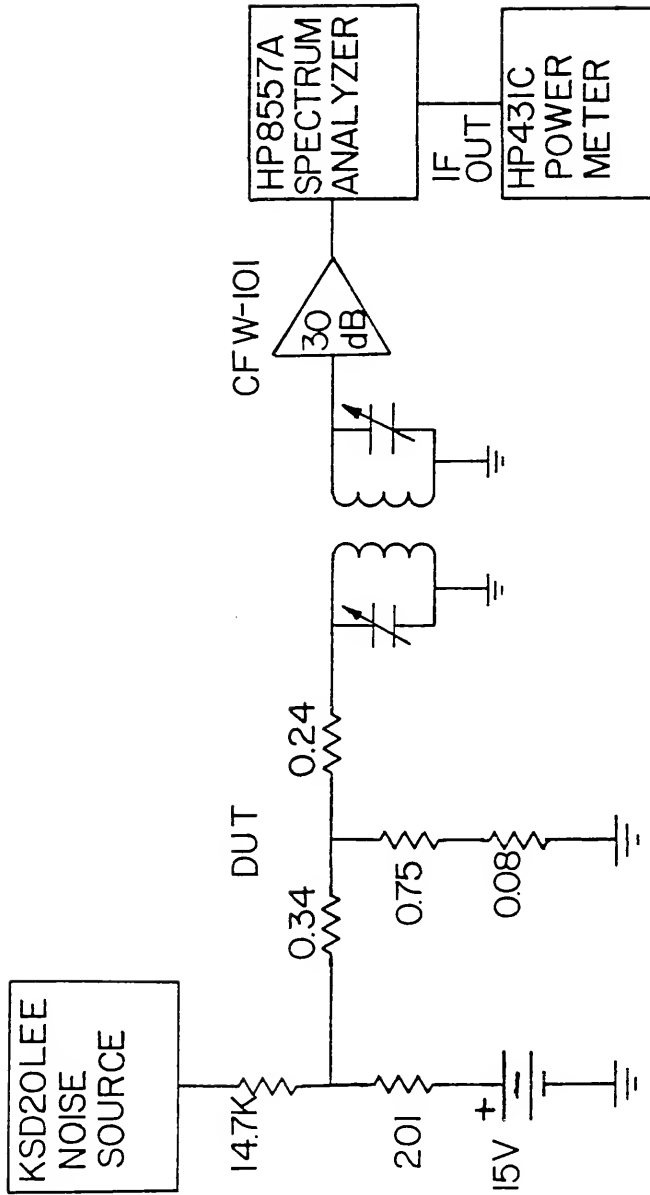
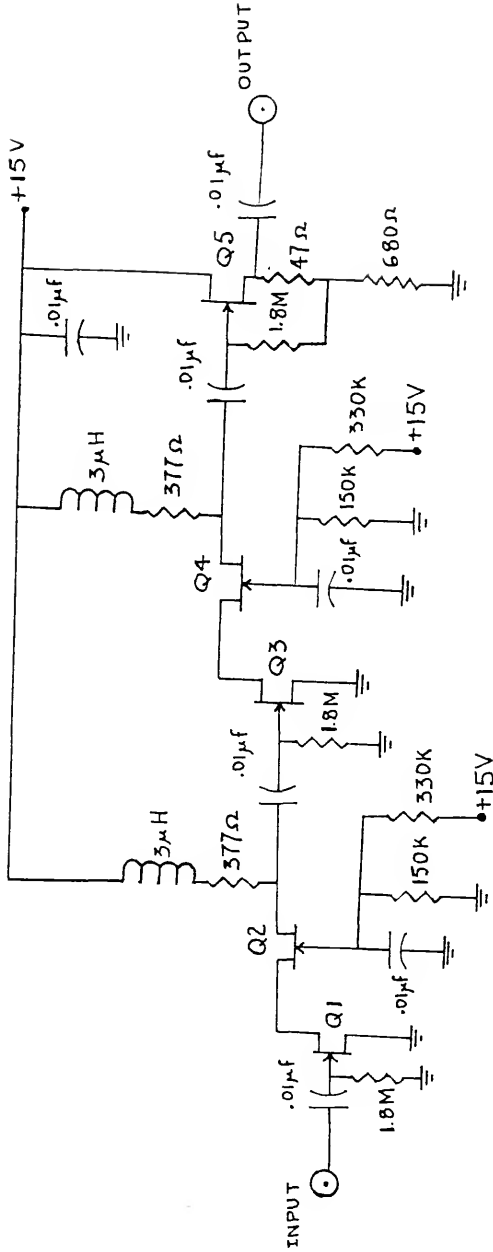Figure 3.18   Radio frequency noise measurement block diagram

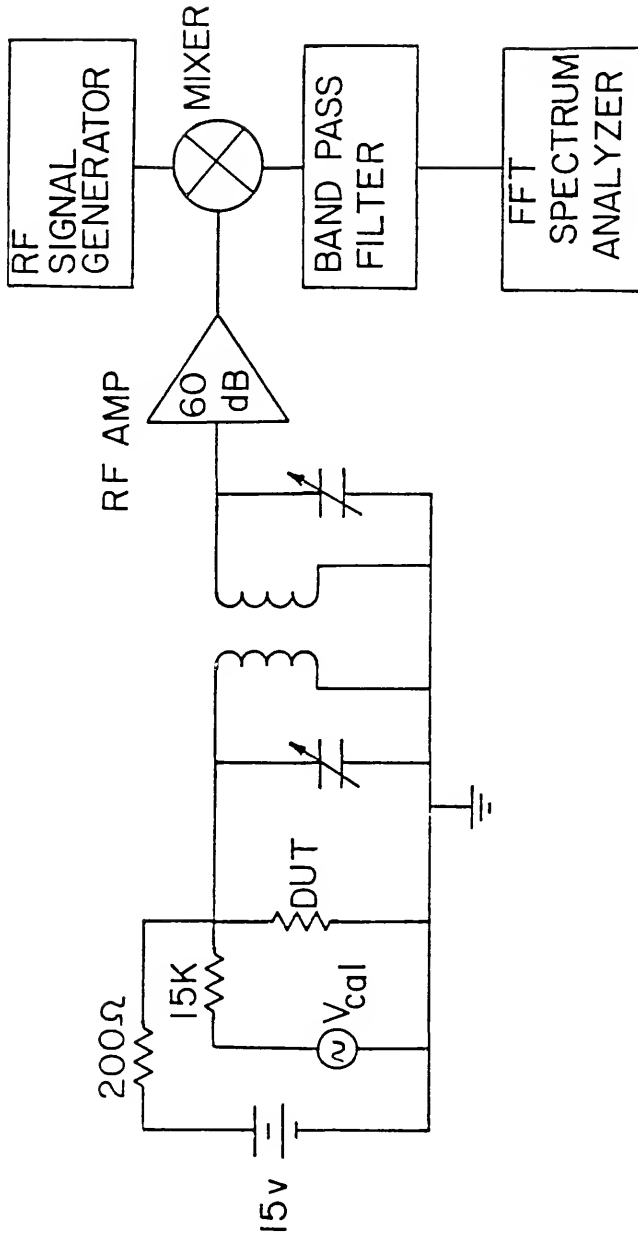Figure 3.19   Radio frequency low-noise preamplifier

Figure 3.20 Radio frequency noise measurement setup using FFT spectrum analyzer

can be used just as easily. The bias and calibration signal are applied as for the conventional RF system. The circuit for the n-type device, using a tuned step-up transformer, is shown. The 60 dB radio frequency preamplifier is actually two of the 30 dB preamplifiers shown in Figure 3.19 in cascade. The large gain is needed to overcome the poor noise performance of the mixer (Mini-Circuits ZAD-1). Using a standard RF signal generator with output amplitude capability of +7 dBm, the mixer has a frequency response of 100 kHz to 500 MHz.

The same signal generator can be used to supply both mixers (correlation setup). Then two 60 dB preamplifiers are used and, if series resistance or unwanted pickup of the step-up transformer is not negligible, two of these also. Feedthrough of local oscillator harmonics may overload the spectrum analyzer at some frequencies if a bandpass filter similar to that shown in Figure 3.21 is not employed. This simple filter had good (90 dB) attenuation to 100 MHz. The bandwidth of a single FFT bin of the spectrum analyzer was extremely small compared to the frequencies of interest, causing significant inaccuracy. To reduce that, a program to average 80% of the bins to synthesize a bandwidth of up to 20 kHz was written. It is shown in the Appendix.
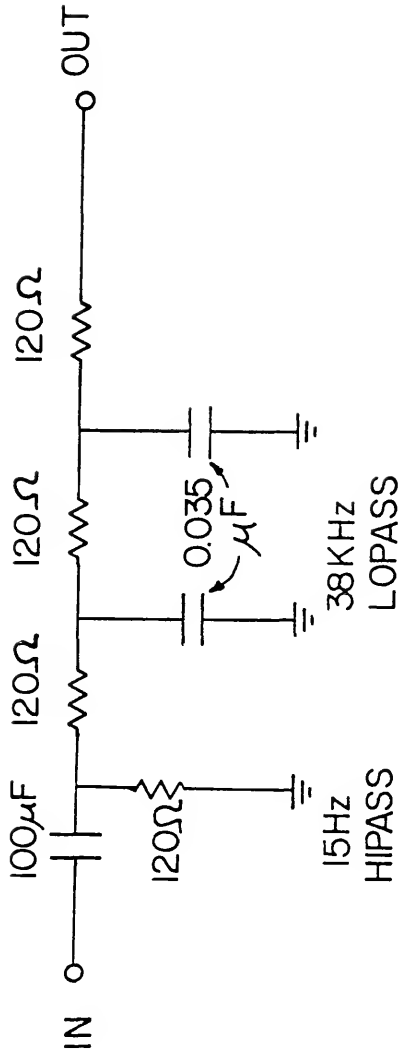
Figure 3.21 Bandpass filter for RF–FFT system

CHAPTER IV
MEASUREMENTS RESULTS

The near-ballistic diode (NBD) is a sandwiched mesa structure of five lightly doped p or n layers, alternating with heavily doped n^+ layers. A not-to-scale sketch of the p-NBD is shown in Figure 4.1. The doping densities of the various regions are 10^{18} cm^{-3} for the n^+ regions, approximately 2×10^{15} cm^{-3} for the n regions, and approximately 6×10^{14} cm^{-3} for the p regions. The diameter of the mesas is 100 μm. The devices were manufactured by molecular beam epitaxy at the Cornell University Submicron Research Facility by Mr. M. Hollis. The mesas have very low-noise ohmic AuGe contacts.

Current-voltage measurements of three types—DC, pulsed DC, and AC—are reported. Also presented are noise spectra versus parameters bias, frequency, and temperature.

4.1 Current-Voltage Characteristics
4.1a The $n^+n^-n^+$ Device

The DC current-voltage characteristics of the 0.4 μm $n^+n^-n^+$ device at room temperature and 77 K are shown in Figure 4.2 In contrast to the device reported in Eastman et al. [1], there is no $\sqrt{V}$ region. The characteristic is linear for both temperatures up to very large bias. Pulse techniques are used for currents greater than 100 mA. The resistance of the active region is 0.75 ohms at room temperature
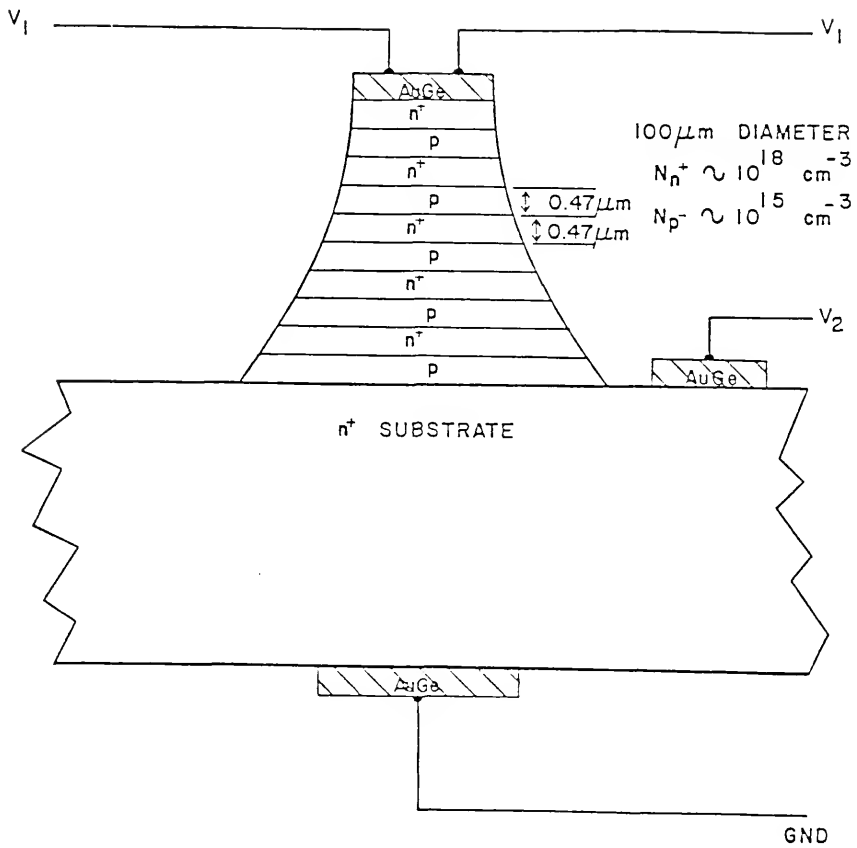
46

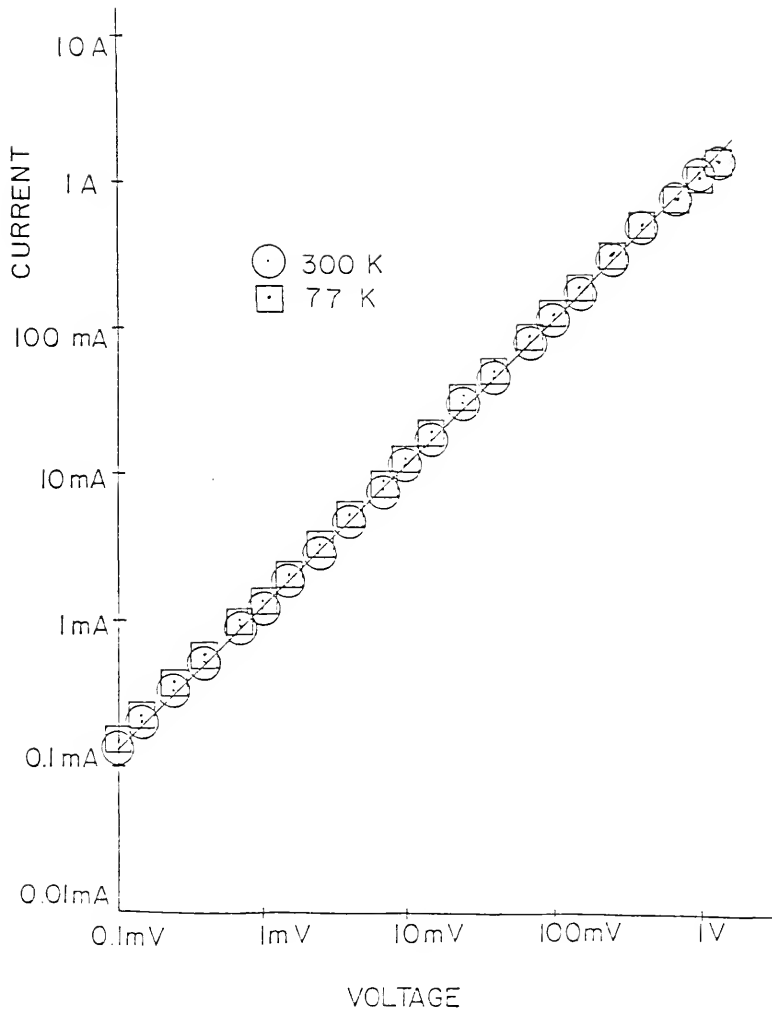Figure 4.1 P-type near-ballistic diode mesa structure

Figure 4.2   DC I-V characteristic of $n^+n^-n^+$ 0.4 μm device

and 0.68 ohms at 77 K. This is confirmed by the AC impedance measurement at 300 K for I_{DC} = 75 mA shown in Figure 4.3. Low-frequency equivalent circuits of the device at room temperature and 77 K are shown in Figures 4.4 and 4.5. The series resistances of the gold wires of the TO-5 can are significant and must be taken into account.

4.1b The $n^+p^-n^+$ Device

Conversely, the $n^+p^-n^+$ structure is quite nonlinear. The DC current-voltage characteristics of the 0.47 μm $n^+p^-n^+$ diode at 300 K and 77 K are shown in Figure 4.6. The device is linear for both temperatures up to about 100 mV. The characteristics then move through transition to a temperature independent high bias regime in which the slope falls off. The maximum slopes in the transition regions are 3 for the 300 K case and 4.5 at 77 K. The low-bias resistances at 300 K and 77 K are 90 ohms and 320 ohms, respectively. The measurements of AC resistance for several bias currents at T = 300 K shown in Figure 4.7 and for T = 77 K shown in Figure 4.8, display no frequency dependence.

To compare the large and small signal resistances more easily, the exponent, β, can be examined where $I = V^{\beta}$. Differentiating both sides and solving for β gives

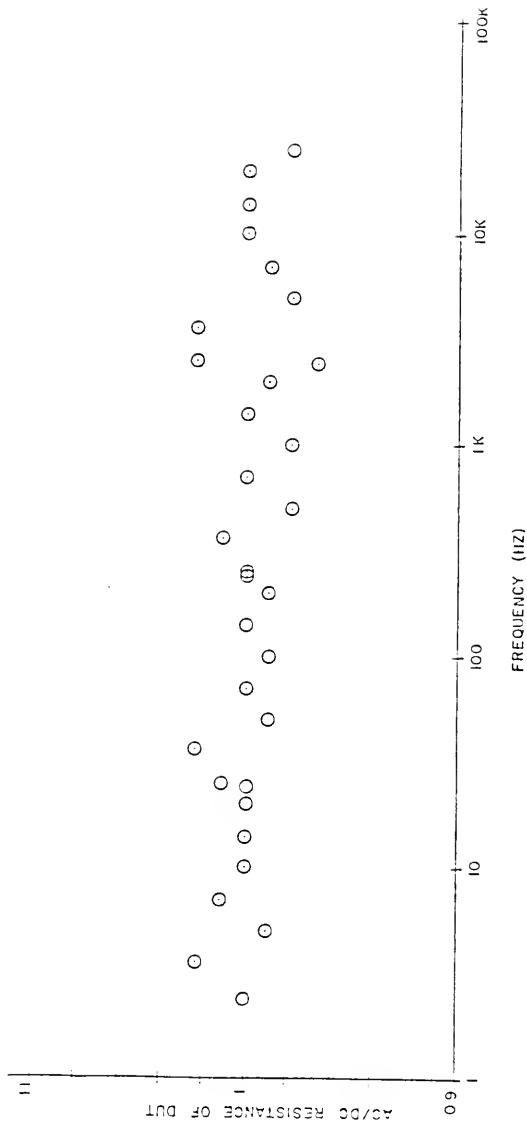$$\beta = \frac{R_{DC}}{R_{AC}} \tag{4.1}$$

Figure 4.3 AC resistance of $n^+n^-n^+$ device versus frequency at room temperature
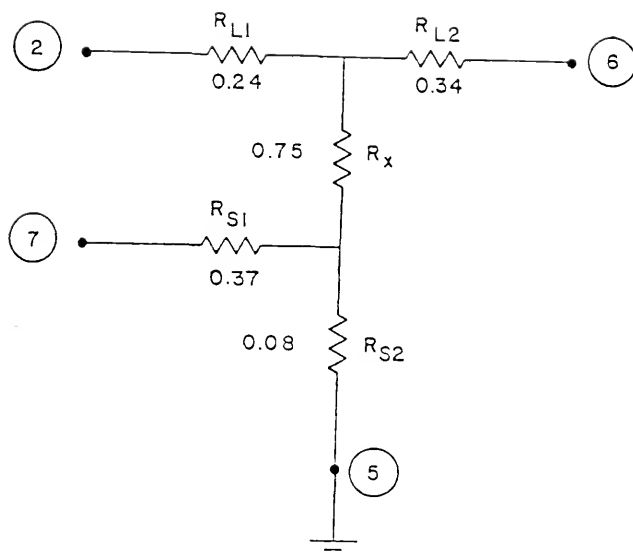
Figure 4.4 Equivalent circuit of $n^+n^-n^+$ structure at 300 K showing parasitic elements
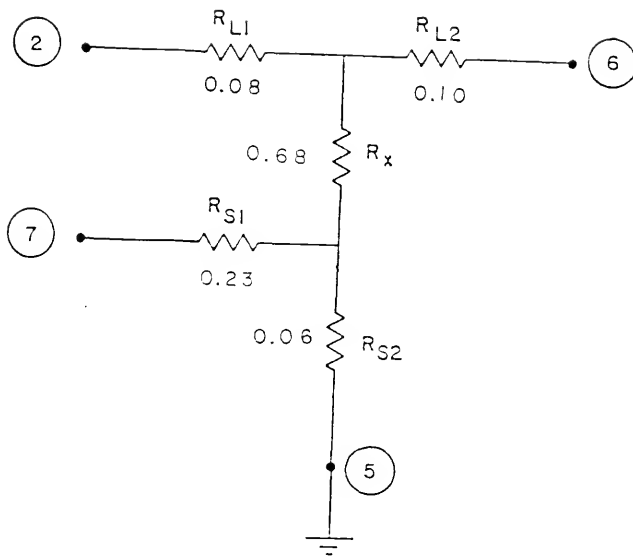
Figure 4.5 Equivalent circuit of $n^+ n^- n^+$ structure at 77 K showing parasitic elements
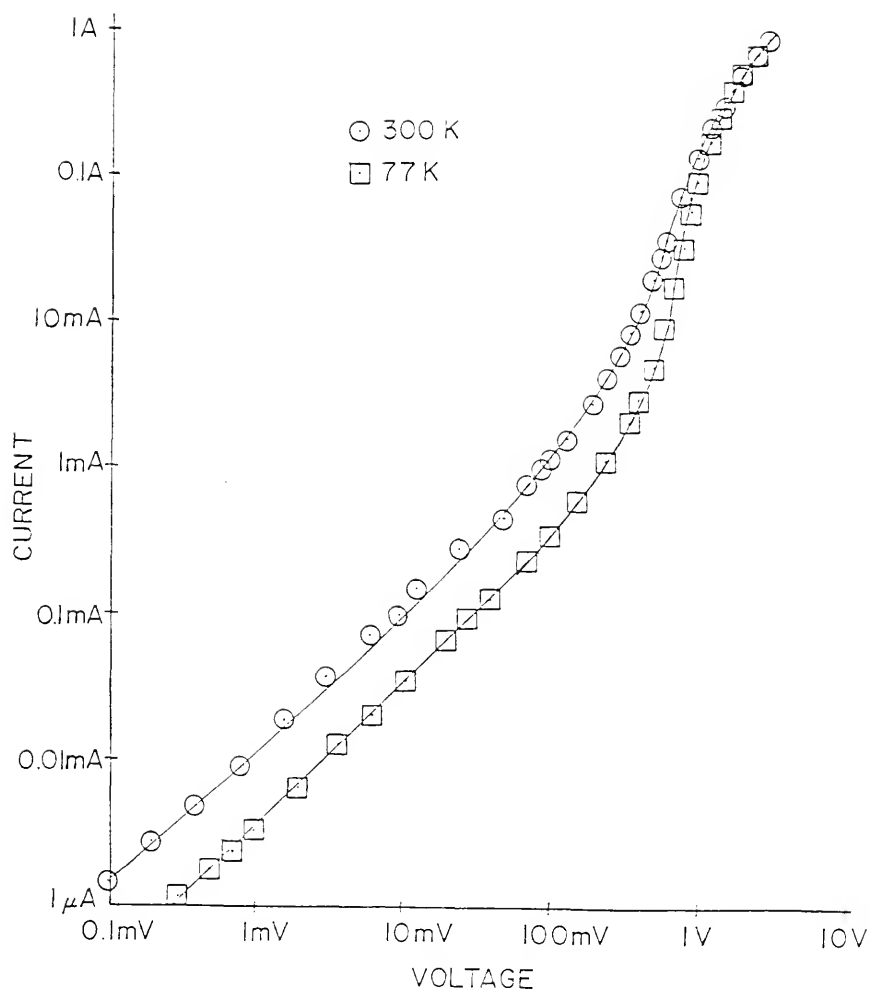
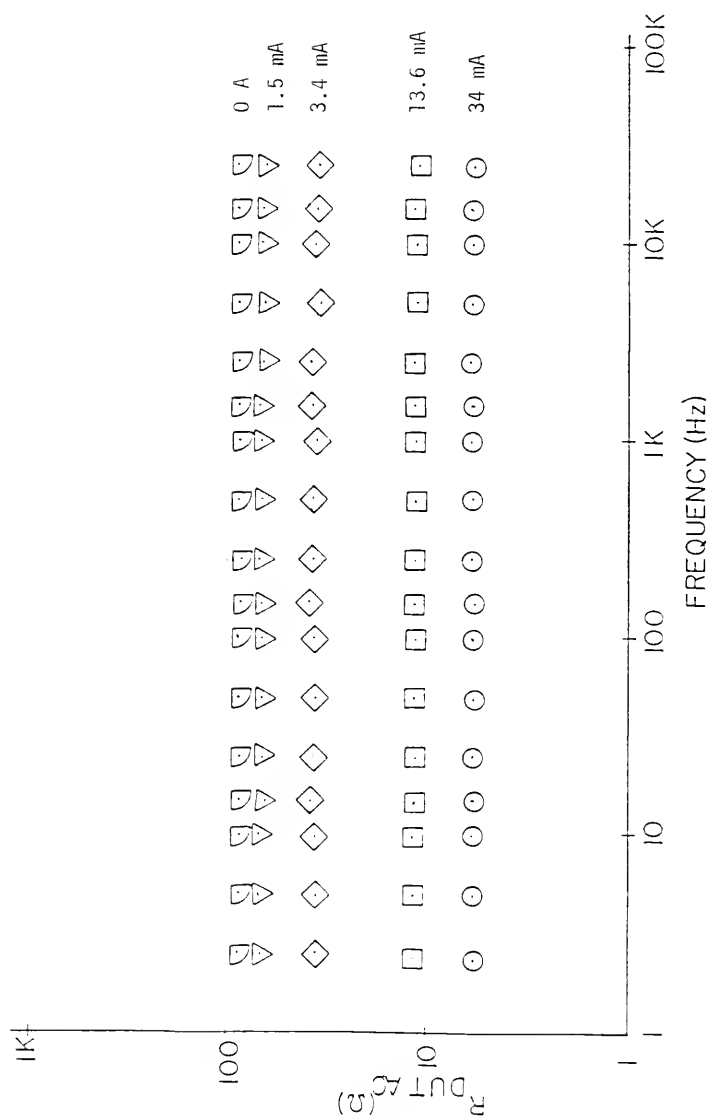Figure 4.6   DC I-V characteristic of $n^+p^-n^+$ 0.47 μm device

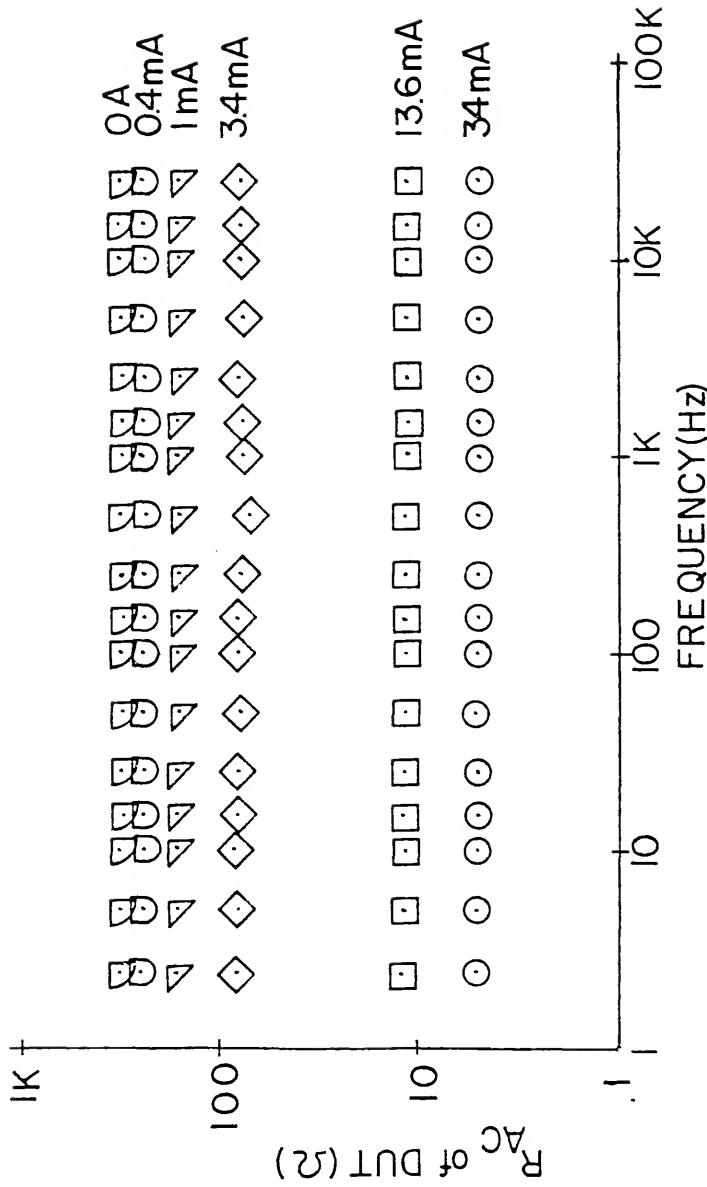Figure 4.7 AC resistance of 0.47 μm $n^+p^-n^+$ NBD at T = 300 K

Figure 4.8 AC resistance of $n^+p^-n^+$ 0.47 μm NBD at $T = 77$ K

This is plotted in Figure 4.9 for small bias up to 34 mA. At higher
bias, pulsed DC but not AC measurements were done. The resistance
falls dramatically at high bias. This is seen more clearly in Figure
4.10 which presents the DC and pulsed DC conductance versus bias
voltage for several temperatures down to 12 K. The large-bias
conductance in the temperature independent regime rises to a limiting
value of about 0.33 Siemens. In the low-bias regime, the conductance
quickly falls from its 300 K value by about a factor of three at 150 K
to 200 K and remains nearly constant for further decreases in tempera-
ture.

4.2 The $n^+p^-n^+$ Device Noise

The $n^+p^-n^+$ 0.47 µm structure exhibited large levels of excess
low-frequency noise. The room temperature noise current spectrum
(less than 25 kHz) for several bias currents is shown in Figure 4.11.
The frequency dependence for all bias currents is about $\left(\frac{1}{f}\right)^{.75}$. In
Figure 4.12 is shown the extension to 32 MHz of the spectra for bias
currents of 100 µA and 1 mA. The 100 µA spectrum is approaching the
thermal level at the high-frequency end. The turnover frequency to
thermal noise occurs in the GHz range for larger bias. Figures 4.13
and 4.14 display the complete spectra versus frequency for bias currents
of 34 mA and 68 mA, respectively. Both show slopes of -0.77 over many
decades. No turnover frequency to a different slope is found. These
spectra represent measurements in the low-bias regime and transition
region. Measurement in the high-bias regime requires pulsed techniques.
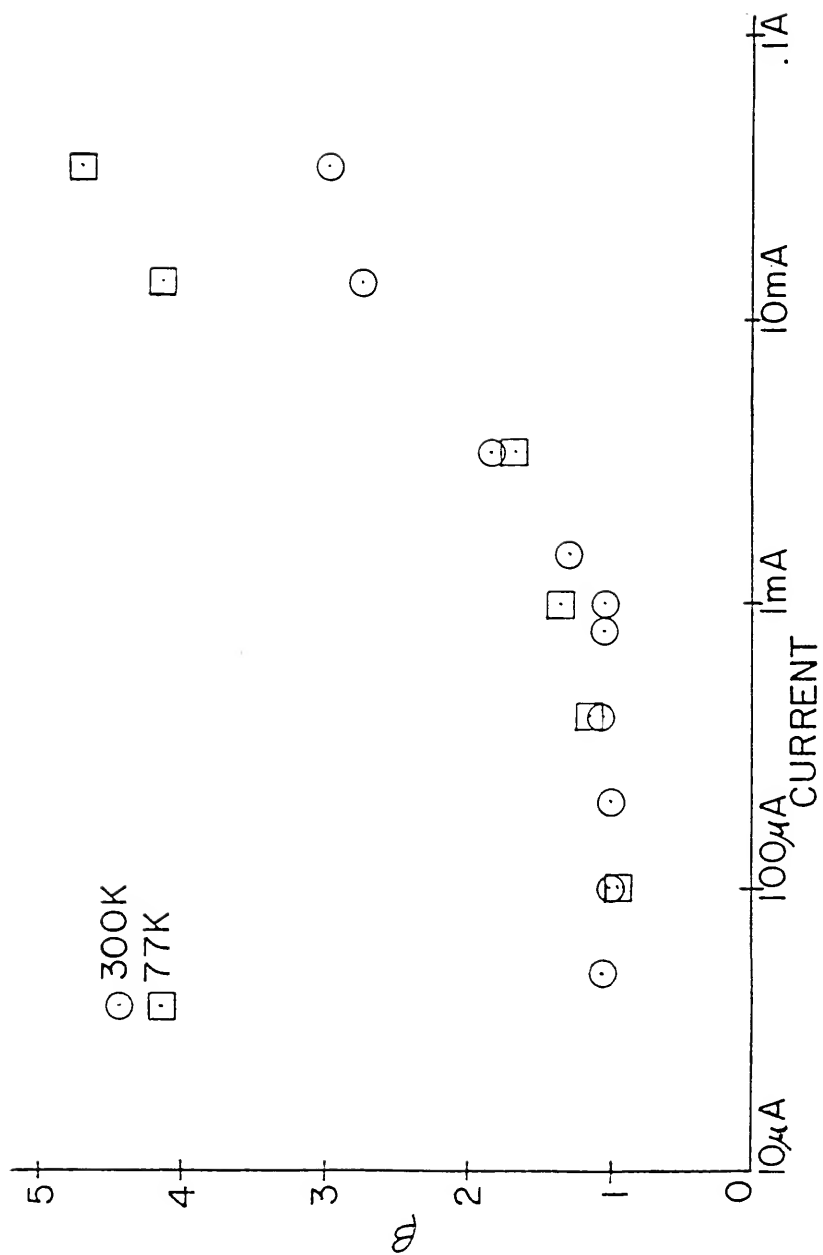
Figure 4.9   Beta versus current at 300 K and 77 K

58
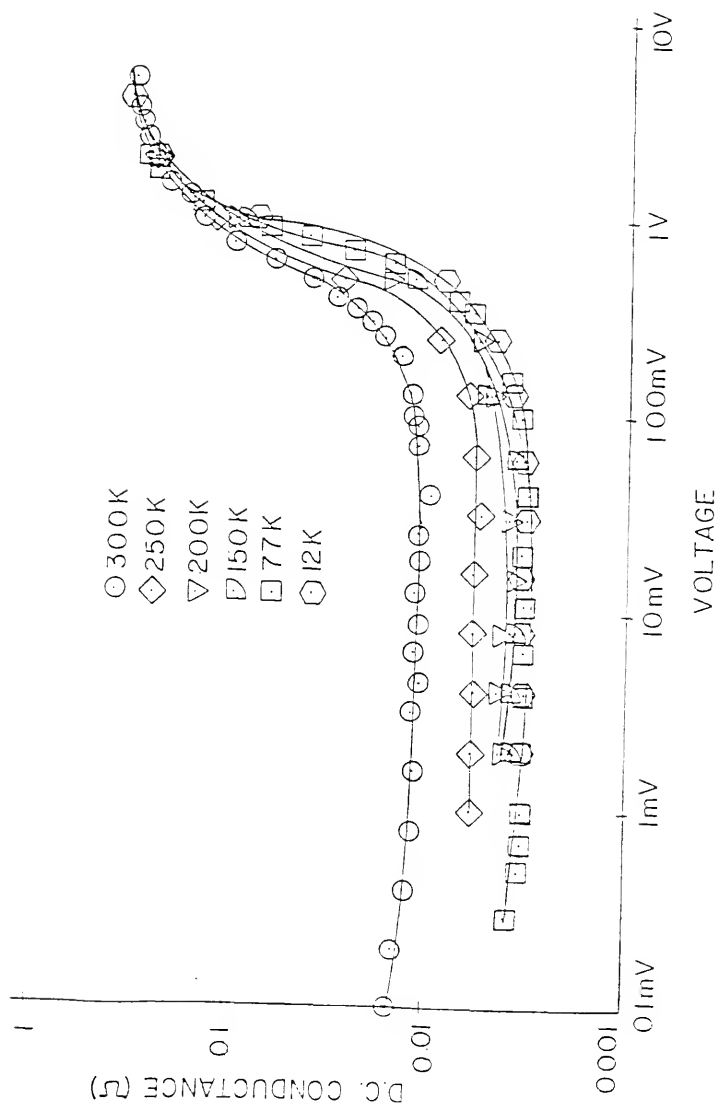
Figure 4.10 DC conductance versus bias voltage for 0.47 μm n$^+$ n$^-$ p$^-$ n$^+$ device at several temperatures
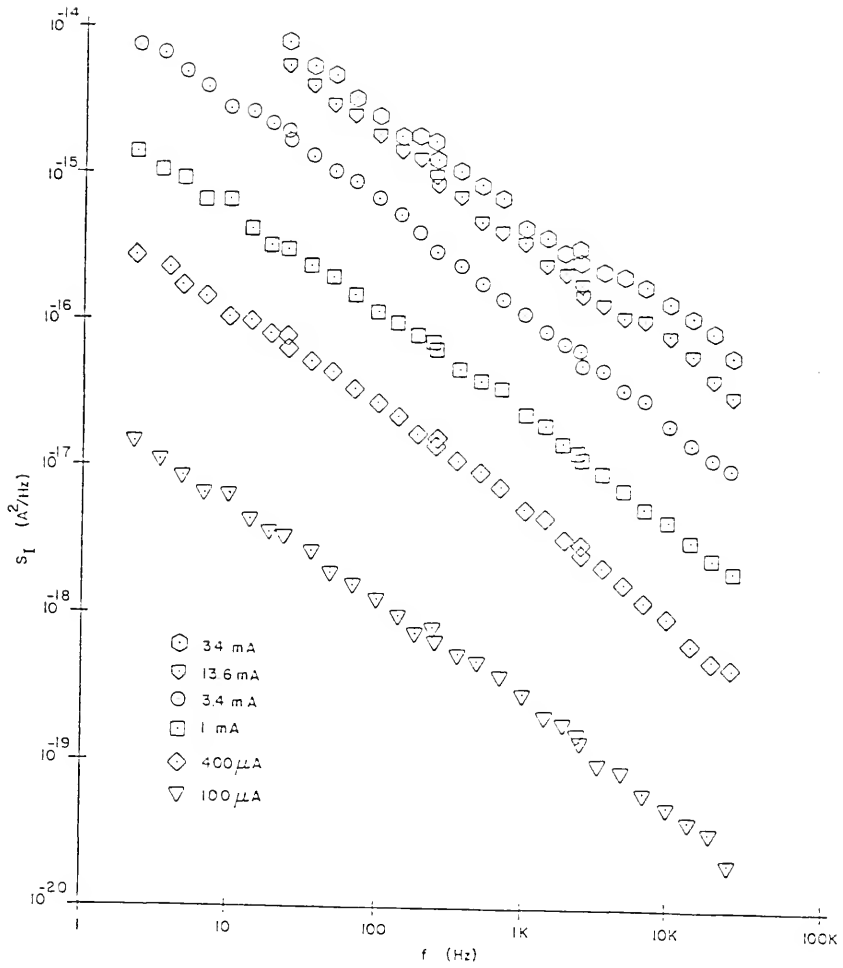
Figure 4.11 Low-frequency p-NBD room temperature current noise spectra
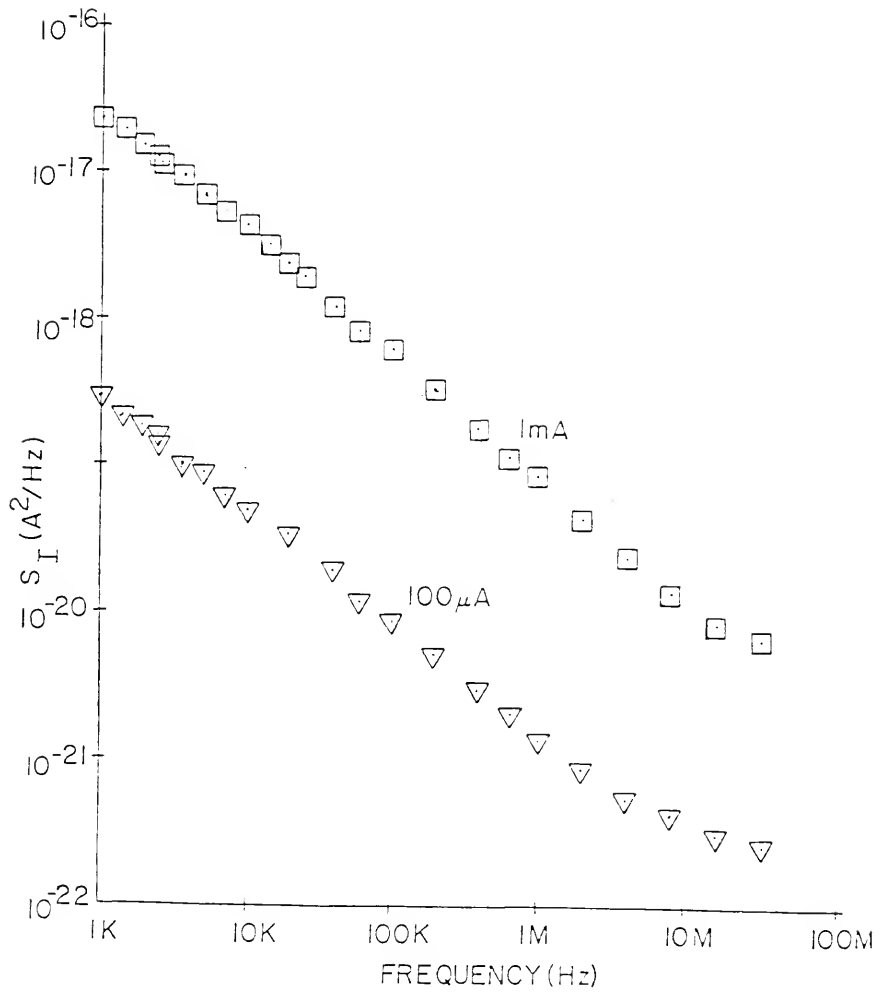
Figure 4.12 Current noise of 0.47 μm $n^+p^-n^+$ NBD at T = 300 K for
I = 100 μA and 1 mA

Figure 4.13   Current noise of 0.47 μm $n^+ p^- n^+$ NBD at T = 300 K for I = 34 mA

Figure 4.14   Current noise of 0.47 μm $n^+ p^- n^+$ NBD at T = 300 K for I = 68 nA

The room temperature current noise at 100 Hz is plotted versus bias current in Figure 4.15. There is an I^2 dependence at lower currents up to a few mA. At higher bias the noise increases less fast. The deviation from I^2 behavior appears to coincide with the transition region.

The low-frequency current noise spectra at 77 K for several bias currents are shown in Figure 4.16. The levels of excess low-frequency noise are again large. The slopes are somewhat steeper than for the room temperature case, being approximately -0.85. Figure 4.17 displays the current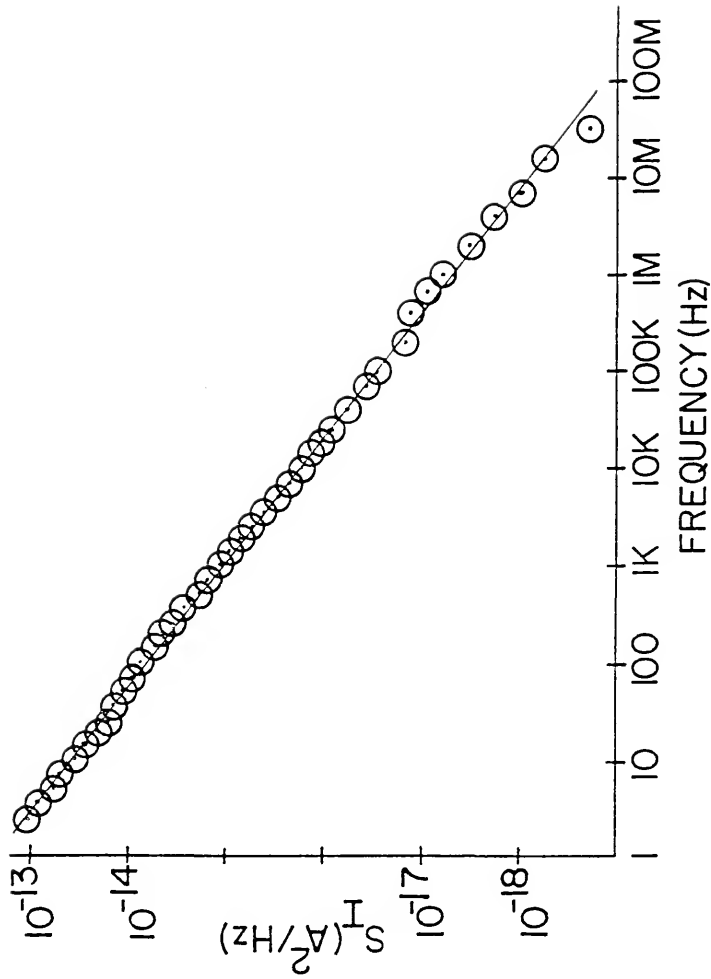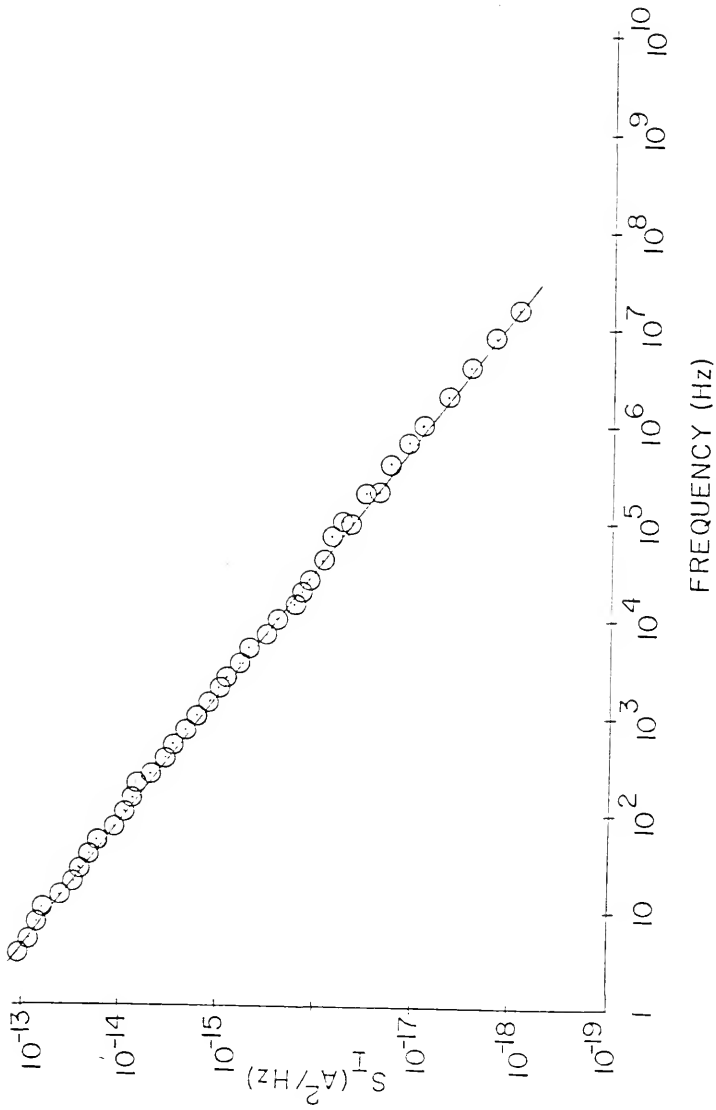 noise at 100 Hz versus bias. Again, I^2 dependence in the low-bias regime with a fall-off in the transition region is observed.

The temperature dependence of the noise in the low-bias regime was investigated further. The low-frequency small bias (100 μA) noise spectra were measured for several temperatures (300 K, 250 K, 200 K, 150 K, 77 K, and 12 K) down to 12 K as shown in Figure 4.18. The magnitude increases with decreasing temperature down to about 200 K. Thereafter, further lowering of the temperature does not affect the magnitude very much, but the slope becomes more closely 1/f. The other temperatures are not plotted since they only obscure the figure. At 12 K, the slope is fully 1/f as shown in Figure 4.19.

4.3 The $n^+n^-n^+$ Device Noise

The magnitudes of the noise levels of the 0.4 μm $n^+n^-n^+$ structure, both thermal and excess low frequency, are very small. The current noise spectra for several bias currents at room temperature is
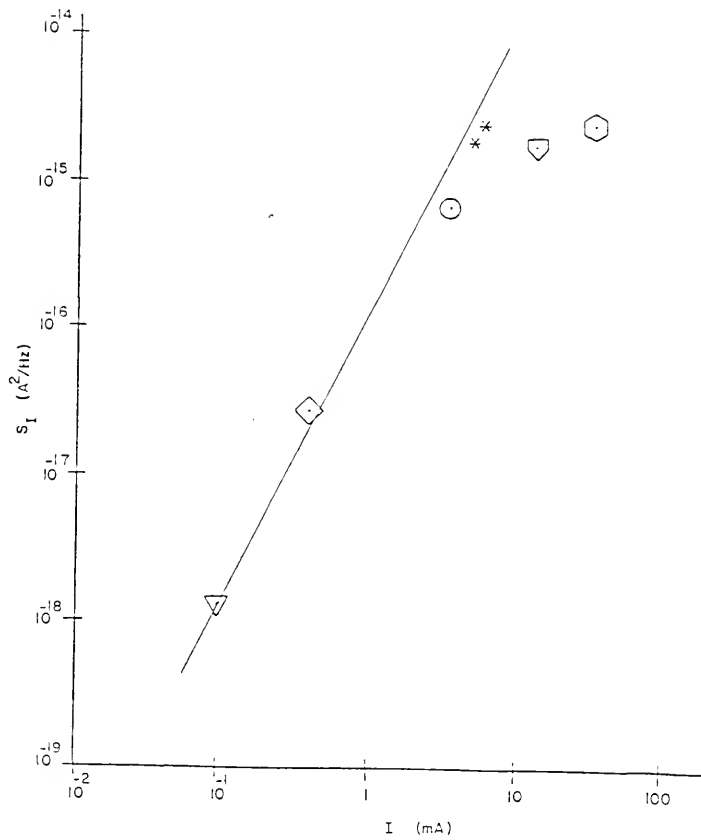
Figure 4.15 Current noise at 100 Hz versus bias current for p-NBD
at T = 300 K
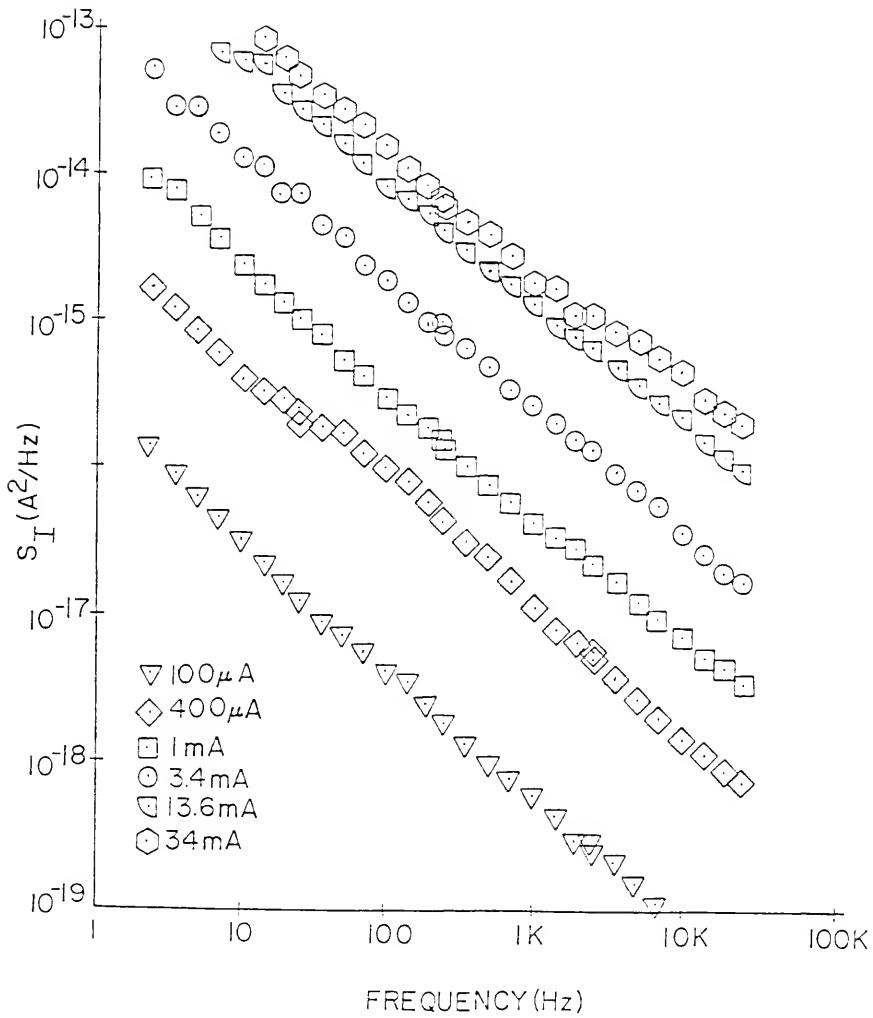
Figure 4.16   Current noise of p-NBD at T = 77 K
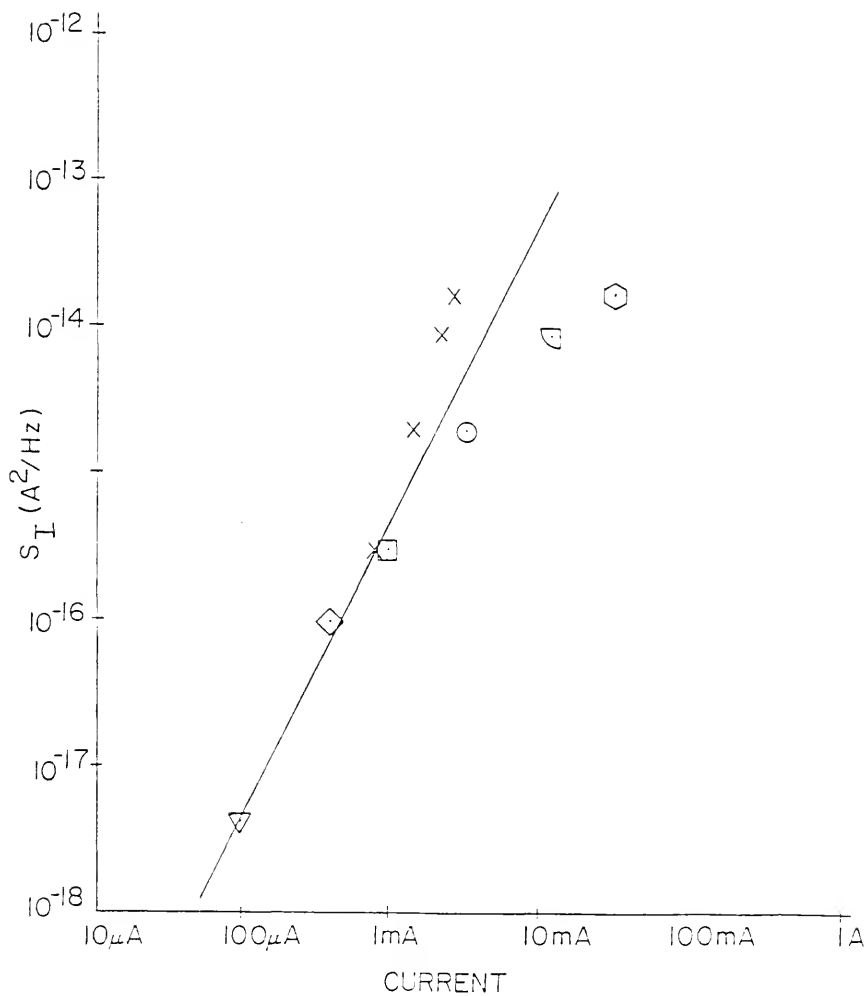
Figure 4.17 Current noise versus current of the p-NBD for f = 100 Hz
and T = 77 K
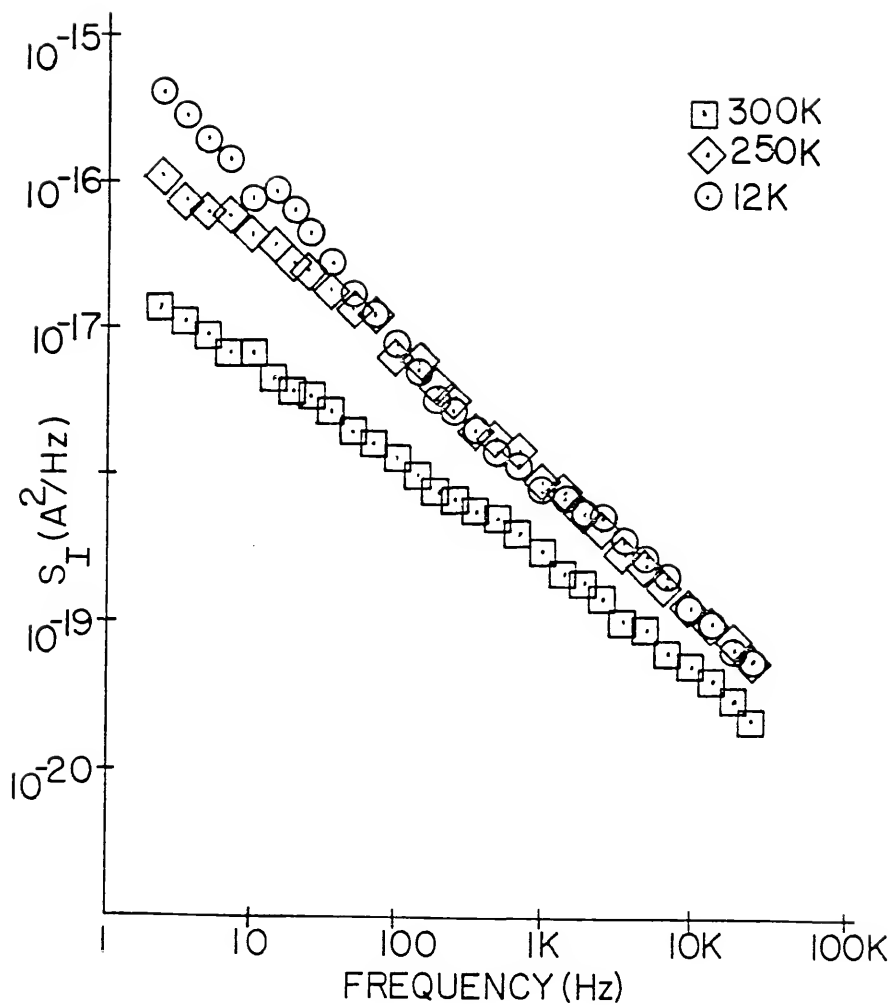
Figure 4.18 Current noise of $n^+p^-n^+$ diode for I = 100 μA and three temperatures
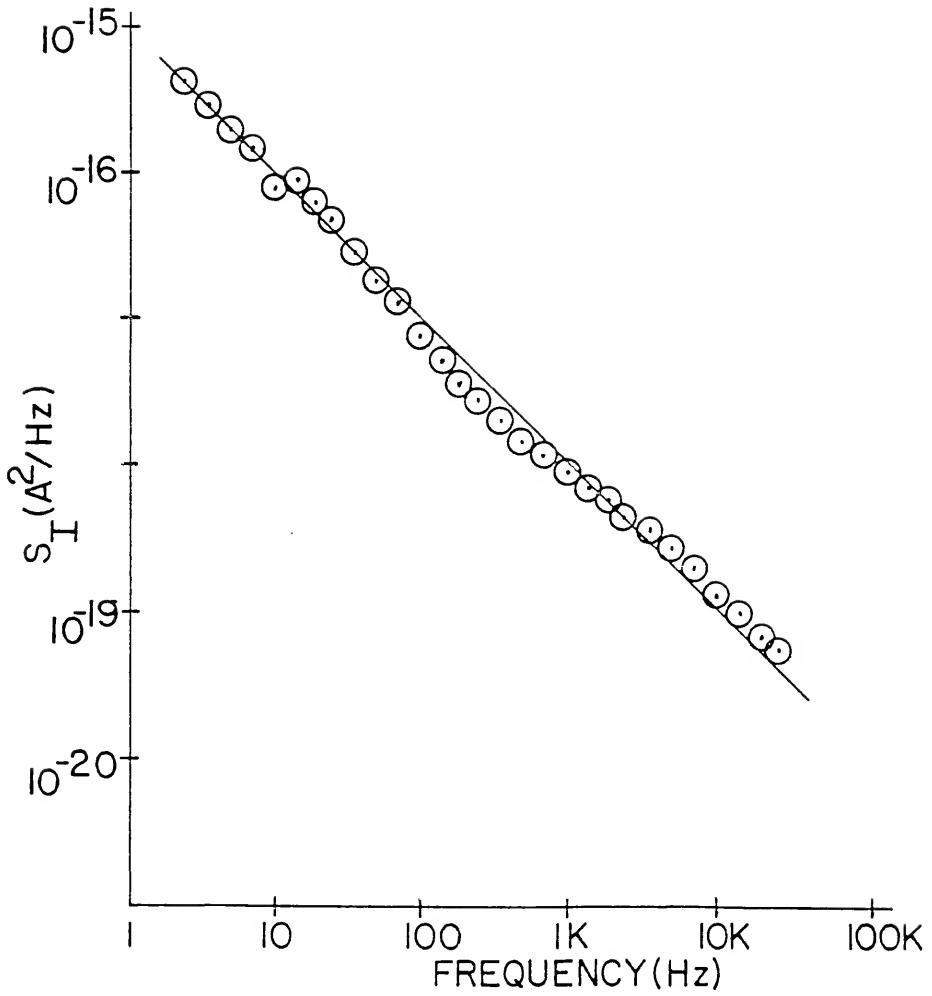
Figure 4.19 Current noise of $n^+p^-n^+$ diode at T = 12 K and I_{DC} = 100 μA

shown in Figure 4.20. Thermal levels and excess low-frequency noise for some levels of bias can be seen. The frequency dependence of the low-frequency noise is 1/f. The spectra from 1 to 25 kHz with the 1/f levels subtracted is shown in Figure 4.21. The lower three bias currents result in approximately thermal noise. There is still excess noise for 75 mA, however. Therefore, a spot noise measurement at 500 kHz for that bias was done. Less than 4% deviation from the thermal level was found. Values at 10 Hz obtained from the straight line approximations to the 1/f noise are plotted versus bias current in Figure 4.22. The expected behavior for 1/f noise, $S_I \sim I^2$ is well satisfied.

Spectra for T = 77 K and the same bias currents are plotted in Figure 4.23. Excess low-frequency noise is found for all current levels. The noise in the thermal region is difficult to determine accurately because the expected value for full thermal noise ($\sim 0.17 \ \Omega$) is below the background noise of even the correlation setup. Also, for some bias currents, the noise is not yet flat at these frequencies. The 1/f noise at 10 Hz is plotted versus bias in Figure 4.24. Again, the I^2 dependence of the magnitude is found.
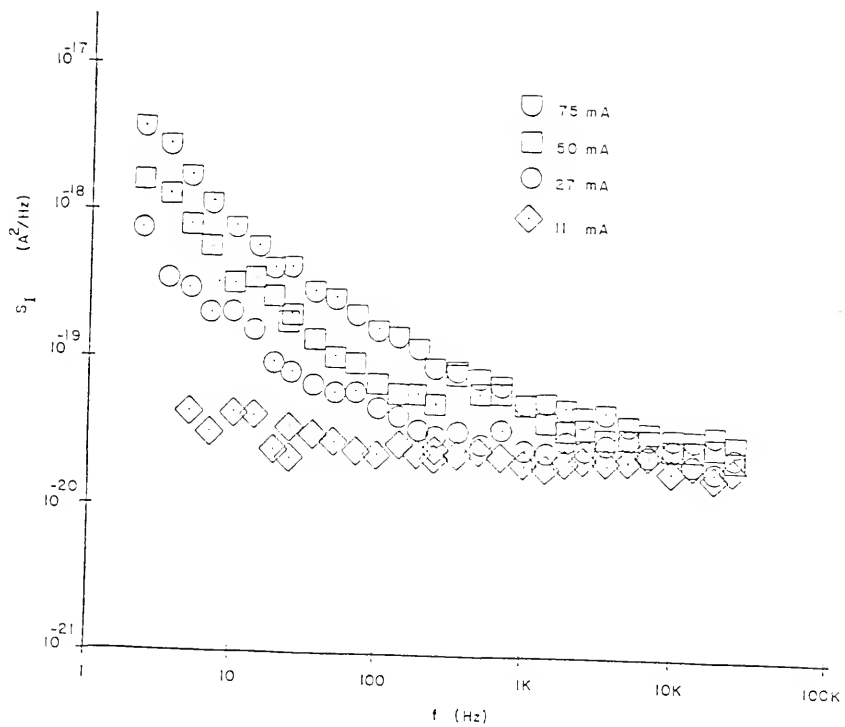
Figure 4.20   Current noise spectra of $n^+n^-n^+$, 0.4 μm NBD at T = 300 K
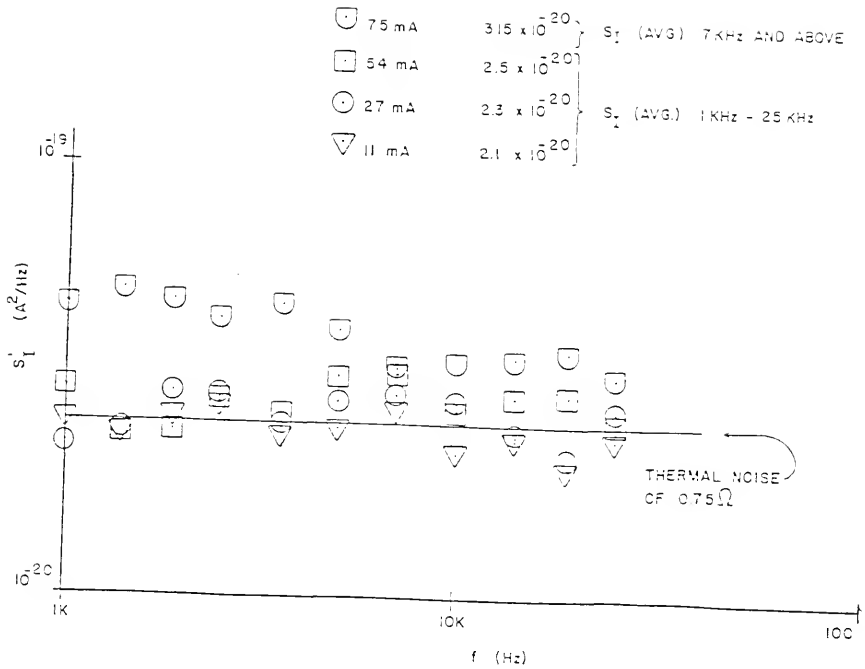
Figure 4.21   Thermal (-like) noise of $n^+n^-n^+$ device
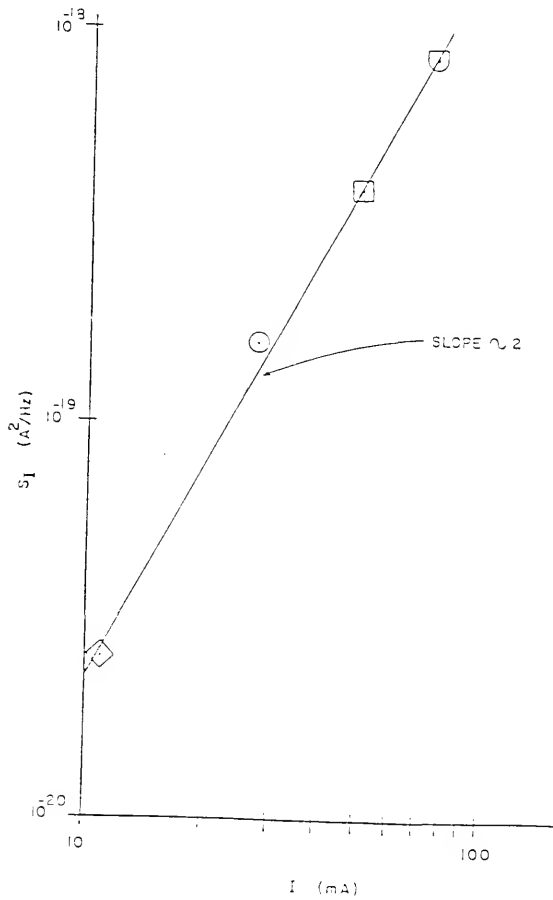
Figure 4.22 Excess 1/f noise of $n^+n^-n^+$ device versus current
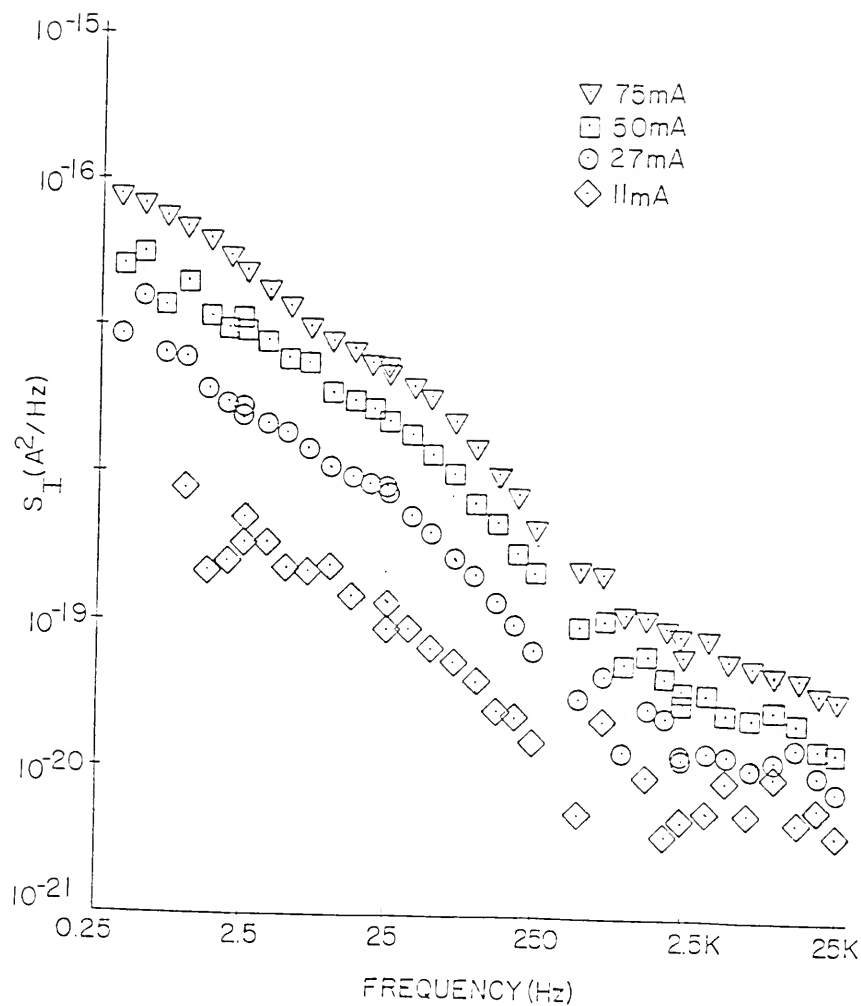
Figure 4.23   Current noise of 0.4 μm n-NBD at T = 77 K
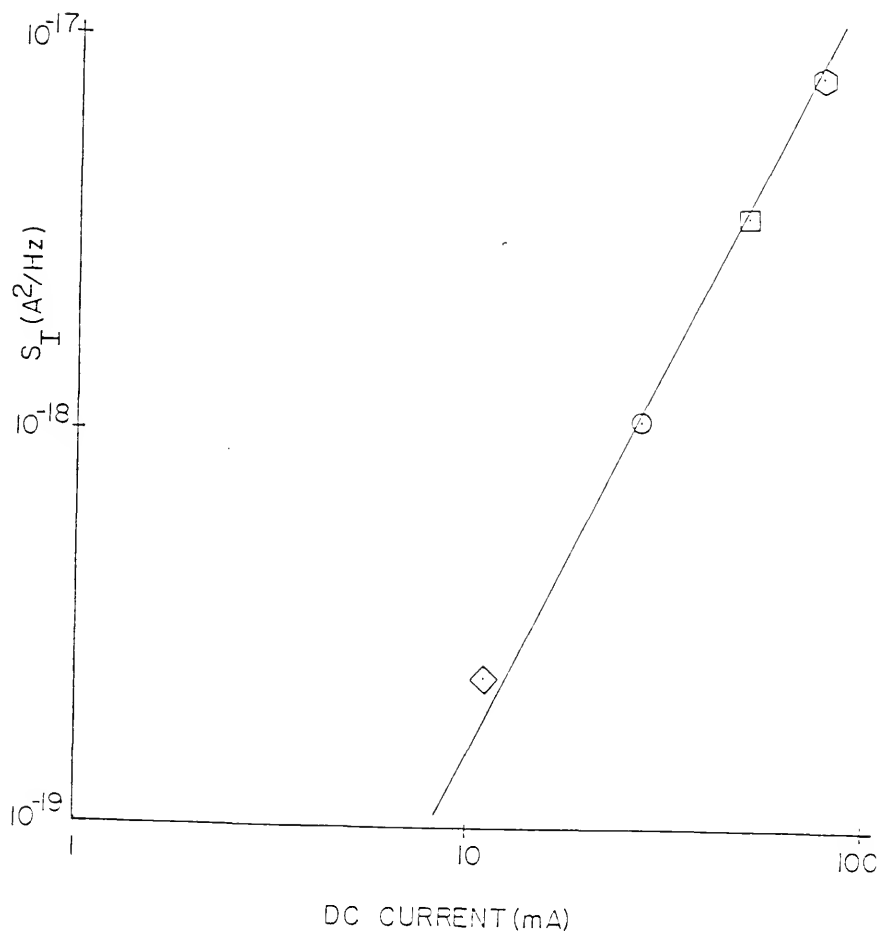
Figure 4.24 S_I of n-NBD at 10 Hz versus bias current for T = 77 K

CHAPTER V
DISCUSSION OF EXPERIMENTAL RESULTS

5.1   The $n^+n^-n^+$ Device

5.1a   Current-Voltage Characteristic and Impedance

The I-V characteristic of the n-type device is seen from
Figure 4.2 to be linear for bias voltages up to about 1 volt and
currents up to about 1 amp for both room temperature and 77 K.   An
attempt to apply pulses at higher bias resulted in melting the gold
bonding wire at the top of the mesa.   Higher bias was desired since a
slight nonlinearity appears at currents greater than 1 amp.   Neverthe-
less, 1 amp corresponds to a current density of 12,800 A/cm^2.   No $V^{1/2}$
or $V^{3/2}$ dependence is found which suggests that theories with these
results are not adequate.

Similarly, the collision-dominated Mott-Gurney theory which
predicts V^2 current dependence at high currents does not apply.
Indeed, sublinear current dependence at high bias seems to be indicated
by the sparse data.   The more realistic theory of Holden and Debney
[12]   gives a high-bias current dependence of $V^{1.14}$ for a 0.5 µm device
where collisions are neglected.   At lower bias, their result appears to
be somewhat sublinear, similar to the $V^{1/2}$ region of Shur and Eastman's [2]
theory.   The theory of van der Ziel et al. [9] gives linear behavior
for small bias.   They include spillover from the highly doped regions

75

and calculate separately the mobilities due to diffusion-drift and thermionic emission. Setting the calculated and measured values of resistance at room temperature equal and solving for the diameter of the mesa gives a 96 μm diameter which is very close to the reported value of 100 μm. At 77 K, the measured value decreases 10%, the calculated value decreases 23%. The impedance is purely resistive at these frequencies.

5.1b Excess 1/f Noise

In the 1/f noise region, we would like to apply Hooge's empirical formula [18] which is Equation (2.12). For mesa structures or nonhomogenous samples [19], Equation (2.13) replaces it and is correct whether or not the transport is ballistic.

In a ballistic or near-ballistic device, many carriers do not undergo any collisions at all. This is in contrast with a typical semiconductor device in which every carrier collides many times. Hooge's formula was developed for the second case, requiring that N, the number of carriers in Equation (2.12) can be determined. In the near-ballistic case, it is desired to exclude those carriers which are transported ballistically, including only those that contribute to the noise. This can be very difficult. Therefore, an alternative expression to describe "noisiness," avoiding this problem, will also be used. Noisiness is described as $(S_{\Delta I}(f)f)/I^2$ which is still dimensionless unless the spectral slope is not -1. Substituting values gives, at 300 K,

$$\frac{S_{\Delta I}(f)f}{I^2} \simeq 1.6 \times 10^{-15} \qquad (5.1)$$

and at 77 K,

$$\frac{S_{\Delta I}(f)f}{I^2} \simeq 1.4 \times 10^{-14} \qquad (5.2)$$

If the slope is not -1, then just $(S_{\Delta I}(f)f)/I^2$ can be reported at a specified frequency.

If $n(x) \simeq \bar{n}$ is a reasonable approximation despite the complex nature of $n(x)$, then Equation (2.13) becomes

$$\alpha_{Hb} = \frac{S_{\Delta I}(f)fALm\bar{n}}{I_0^2} \qquad (5.3)$$

where the subscript, b, denotes validity for the ballistic case. If the transport can be characterized by a constant mobility, μ, the measured resistance is

$$R = \frac{m}{q\mu A} \int_0^L \frac{dx}{n(x)} \qquad (5.4)$$

Then, for the collision-dominated case, Hooge's constant becomes

$$\alpha_{Hc} = \frac{S_{\Delta I}(f)f(mL)^2}{I_0^2 q\mu R} \qquad (5.5)$$

Assuming that $\mu_{300K} = 0.74 \frac{m^2}{V-sec}$, $\mu_{77K} = 14 \frac{m^2}{V-sec}$, $A = 7.9 \times 10^9 \, m^2$, and $\bar{n} = 2 \times 10^{15} \, cm^{-3}$ gives at 300 K,

$$\alpha_{Hc} = 7.2 \times 10^{-8} \tag{5.6}$$

and

$$\alpha_{Hb} = 5 \times 10^{-8} \tag{5.7}$$

At 77 K the values are

$$\alpha_{Hc} = 3.7 \times 10^{-8} \tag{5.8}$$

$$\alpha_{Hb} = 4.5 \times 10^{-7} \tag{5.9}$$

These values are five orders of magnitude smaller than the value reported by Hooge et al. [16] for n-type bulk GaAs of 6×10^{-3}. Thus the number of collisions for this device is very small. The remaining collisions involve polar optical phonon emission typically with a very small deflection angle [1], θ. Handel's [24] quantum theory of 1/f noise indicates that the magnitude of the relative 1/f noise goes as $\sin^2 \frac{1}{2}\theta$ so that the residual noise is very low.

Comparing the ballistic and collision-limited case temperature dependence of α_H suggests that the device is not purely ballistic at either temperature since the low temperature α_{Hb} is nine times larger than the value at room temperature. Further, the diffusion-drift resistance calculated by van der Ziel et al. [9] is larger than the

thermionic emission resistance for both temperatures. However, the values are within a factor of two of each other. The very low value of α_H suggests near-ballistic transport.

5.1c High-Frequency Noise

The device exhibits nearly 100% thermal noise at all currents to 75 mA if sufficiently high frequencies are attained. This current corresponds to a current density of 960 A/cm^2. There is no detailed theory for the noise as yet developed for all applied bias, just the preliminary calculations of van der Ziel and Bosman [14,15]. For the collision-dominated space-charge-limited diode at low bias, the noise is due to diffusion noise sources which transform via Einstein's relation to $4kT/R_x$. At high bias for which the Mott-Gurney law ($I \sim V^2$) applies, the noise becomes $8kT/R_x$ where $R_x = \frac{dV}{dI}$. For a ballistic device the noise is due to shot noise. At sufficiently high bias where space charge effects dominate, correlations between current components due to fluctuations in the potential minimum caused by the space charge lead to subthermal noise.

In order to differentiate between the two models, high bias must be achieved. Our measurements have found no deviations from thermal noise. One possible reason for this is that the current density of 960 A/cm^2 is insufficient. Another is that the device is operating in between the two regimes as suggested by the 1/f measurements so that extreme bias may be required to see which effect dominates.

5.2 The $n^+p^-n^+$ Device

5.2a Current-Voltage Characteristic and Impedance

The $n^+p^-n^+$ device shows substantial nonlinearity. There are two regimes with a transition region in between as shown in Figure 4.10. At low bias, the device is linear with a DC conductance at room temperature 100 times smaller than the n-type device. It decreases with decreasing temperature to a limiting value a factor of 3 below its room temperature value. It reaches this value near 150 K and remains constant thereafter down to 12 K. The high bias regime is temperature independent and is also linear with a large conductance 4 times less than the n-type device.

Due to the thinness of p-regions and the large doping density of the n^+ regions, the spillover of electrons into the p-regions is not very different than for the n-type diode case [9]. Then current flow should be by nearly ballistic electron emission through the potential minimum. The resulting characteristic should be linear with a large conductance and nearly temperature independent. This appears to be a good model for the high bias regime. At low bias, the model fails, however. One possible reason for this is that enough holes remain in the p-region to control the transport ambipolarly. The details of such an effect are unclear, but a qualitative description by Dr. C. M. Van Vliet follows. The motion is not strictly ambipolar, since there is space charge, as indicated by the presence of the potential minimum [9], which even for V = 0 can be computed from Poisson's equation. Therefore, near the potential minimum the excess electron

charge is small. Roughly speaking, only ambipolar pairs with energies within kT of the potential minimum are able to cross the minimum. If the injected carrier density Δn is less than p at a point (labeled x') approximately kT greater in energy than the minimum on the injecting side, then the current will be ambipolar (instead of ballistic). Clearly, with decreasing T, p(x') decreases. Thus, with decreasing T the ambipolar current decreases, and the transition to ballistic behavior—which is independent of T—sets in at lower bias. The I/V versus V characteristic is therefore as shown in Figure 4.10.

In any case, assuming that holes control the mobility for low bias, and electrons at high bias gives a factor of 21 change in the conductance at room temperature since typical values are $\mu_n \sim 8,500 \frac{cm^2}{V\text{-}sec}$ and $\mu_p \sim 400$ cm^2/V-sec [25]. There still remains to be explained the factor of 4 difference between the n-device conductance and the high bias p-device conductance. The potential barrier is larger in the p-type device [26]. In the p^- region, Poisson's equation is

$$\frac{d^2\psi}{dx^2} = \frac{q(n + N_a - p)}{\varepsilon\varepsilon_0} \tag{5.10}$$

where $\psi(x)$ is the potential, $n(x)$ the electron density, $p(x)$ the hole density, N_a the acceptor density, and $\varepsilon\varepsilon_0$ the dielectric constant. For the n-device in the n^- region

$$\frac{d^2\psi}{dx^2} = \frac{q(n - N_d)}{\varepsilon\varepsilon_0} \tag{5.11}$$

If $p(x)$ is assumed negligible due to electron spillover, then

$$\left(\frac{d^2\psi}{dx^2}\right)_{p-} > \left(\frac{d^2\psi}{dx^2}\right)_{n-} \tag{5.12}$$

so that the n-device barrier is smaller. The above model of ambipolar collision-dominated flow at low bias and near-ballistic electron emission at high bias gives a qualitative explanation of the experimental data.

5.2b Noise

The $n^+p^-n^+$ device showed much larger levels of noise than the n-type device. The frequency dependence of the spectra for all measured currents is about $(1/f)^{.75}$ for all measured bias currents at room temperature. Then Hooge's parameter is not well defined since it is not dimensionless (unless the slope is -1) and depends on frequency. The noisiness at 10 Hz and 100 μA is

$$\frac{S_{\Delta I}(f)f}{I^2} \simeq 6 \times 10^{-9} \tag{5.13}$$

This is about 4×10^6 times the n-type device value. The spectral slopes do not change in the transition from low to high bias. The magnitude of the noise does fall off at high bias from the I^2 dependence seen at low bias, however. This suggests that the noise is associated with the low bias transport mechanism and that the high bias mechanism

is much less noisy. That is in good agreement with the conjecture of ambipolarly governed flow at low bias and near-ballistic flow at high bias. The -0.75 slope is not common although van de Roer [27] has also found spectra going slower than 1/f in 6 μm $p^+n^-p^+$ punch-through diodes. The spectra become more closely 1/f as temperature decreases. At 77 K the slope is -0.85 which is common for intermediate temperatures down to 12 K. The magnitude of the noise is

$$\frac{S_{\Delta I}(f)f}{I^2} \simeq 3.3 \times 10^{-8} \tag{5.14}$$

at 10 Hz and 100 μA. Finally, at 12 K, the slope is fully -1 with magnitude

$$\frac{S_{\Delta I}(f)f}{I^2} \simeq 10^{-7} \tag{5.15}$$

at 10 Hz and 100 μA. The explanation of this temperature-dependent slope is unclear.

CHAPTER VI
CONCLUSIONS AND RECOMMENDATIONS
FOR FURTHER WORK

6.1 The $n^+n^-n^+$ Device

The $n^+n^-n^+$ device is nearly ballistic. Carrier transport is
by both thermionic emission and by collision-based diffusion-drift.
Neither process can be neglected in a physical model. For the I-V
characteristic, it is desired to calculate $n(x)$, $\psi(x)$, and $J(V)$ for
any applied bias, expanding on the calculations of van der Ziel et al.
[9] for small V. Alternately, the model of Holden and Debney [12]
should be further developed to investigate the effect of adding col-
lisions to their model. Also the temperature-dependence and the
effects of replacing the Maxwell-Boltzmann velocity distribution by
a Fermi-Dirac distribution should be investigated.

Since nonlinearity in the I-V characteristic appears at high
bias, very fast ($\sim$1 nsec) pulse measurements at yet higher bias
would be very interesting. The mechanism causing this nonlinearity
should be identified.

For the noise, the measured value of α_H found was extremely
low. This is the best confirmation yet that lattice phonon scattering
causes 1/f noise. It would be valuable to repeat the measurement on
other mesas. Perhaps in such small devices Handel's [24] fundamental
theory can be tested.

84

In the thermal noise region, the results were inconclusive, neither subthermal nor greater than thermal noise was found. Perhaps the bias level was not great enough. In that case pulsed noise measurements could be attempted. This may be difficult since the noise is already very low. A detailed and complete noise theory for these devices is desirable, including collision effects and velocity dispersion. A Langevin equation based on the momentum and energy balance equations of Shur and Eastman [5,6] but including the above effects should give accurate results.

6.2 The $n^+p^-n^+$ Device

The p-type device was very intriguing, beginning with the I-V characteristic. At present it is believed that at low bias the carrier transport is ambipolar and collision-limited, centering about the potential minimum. At high bias, the injected electrons overrun the holes and near-ballistic electron flow results similar to the n-type device. The conductance is less because the potential barrier is greater. This model deserves further detailed investigation.

The noise is very large and shows slopes becoming progressively less 1/f as temperature is increased. This interesting characteristic suggests that subtle and complex mechanisms may be taking place that are not well understood yet. To develop a theory that explains these effects would be a great step forward in our knowledge of very small devices. The 1/f noise extends to the GHz range to frequencies greater than our measurment system so that thermal noise measurements have still

to be done. In addition, only these low-bias measurements have been done; pulsed noise measurements in the high-bias regime are underway; they may yield valuable information.

Investigation of this device has led to another novel device [29]. A $p^+n^-p^+$ device with nonlinear characteristics is predicted to have negative differential conductance. At low bias, electron-controlled ambipolar flow should give a large conductance. At larger bias, hole injection takes over with collision-limited flow resulting in a low conductance. The transition region, therefore, should show the negative differential conductance.

APPENDIX
COMPUTER PROGRAMS FOR THE HP 9825

APPENDIX

COMPUTER PROGRAMS FOR THE HP 9825

A.1 Correlation-System Three-Measurement Average

This program calculates equations for the current noise spectral density of a device under test (DUT) using the three-measurement technique. Actually, the magnitude of the calibration signal is also recorded. The program calculates data for eight logarithmically equal-spaced points covering one decade in frequency. It is used with the HP 3582A spectrum analyzer which features a dual-channel Fast Fourier transform algorithm for frequencies from 0.02 Hz to 25 kHz. Many data sets can be averaged to increase the accuracy of the measurement which is described in Chapter III.

```
0: "REPEATED-3 MEASUREMENT CORRELATION SYSTEM":
1: 0→A→B→C→D
2: dim A[24],B[24],C[24],F[8],M[8],S[8],X[8],Q$[1],LS[20]
3: dim M$[8,5];"MP12"→M$[1];"MP18"→M$[2]
4: "MP25"→M$[3];"MP35"→M$[4];"MP50"→M$[5]
5: "MP70"→M$[6];"MP95"→M$[7];"MP125"→M$[8]
6: 12→S[1];18→S[2];25→S[3];35→S[4];50→S[5];70→S[6];95→S[7];125→S[8]
7: ldf 1,A,B,C,D,A[*],B[*],C[*],F[*],M[*]
8: fxd 0;dsp A,B,C,D,F[8];beep;stp
9: flt 3
10: "n"→Q$:ent "DUT ON (y/n)",Q$;if Q$="y";gto "DUTON"
11: "n"→Q$:ent "DUT OFF (y/n)",Q$;if Q$="y";gto "DUTOFF"
12: "n"→Q$:ent "CAL ON (y/n)",Q$;if Q$="y";gto "CALON"
13: "n"→Q$:ent "CAL MAG (y/n)",Q$;if Q$="y";gto "CALMAG"
14: "n"→Q$:ent "CALC NOISE (y/n)",Q$;if Q$="y";gto "NOISE"
15: "n"→Q$:ent "CLEAR DATA FILE (y/n)",Q$;if Q$="y";gto "CLEAR"
16: "DONE":
17: rcf 1,A,B,C,D,A[*],B[*],C[*],F[*],M[*]
18: fxd 0;dsp A,B,C,D;beep
```

```
19: lcl 7i1;end
20: "DUTON":
21: for I=1 to 8;gsb "GET"
22: if A=Ø;X→A[I];Y→B[I];Z→C[I];next I
23: if A≠0;jmp 4
24: (X+A*A[I])/(A+1)→A[I]
25: (Y+A*B[I])/(A+1)→B[I]
26: (Z+A*C[I])/(A+1)→C[I];next I
27: A+1→A;gto "DONE"
28: "DUTOFF":
29: for I=1 to 8;gsb "GET"
30: I+8→J
31: if B=Ø;X→A[J];Y→B[J];Z→C[J];next I
32: if B=Ø;jmp 3
33: (X+B*A[J])/(B+1)→A[J];(Y+B*B[J])/(B+1)→B[J]
34: (Z+B*C[J])/(B+1)→C[J];next I
35: B+1→B;gto "DONE"
36: "CALON":
37: for I=1 to 8;gsb "GET"
38: I+16→J
39: if C=Ø;X→A[J];Y→B[J];Z→C[J];next I
40: if C=Ø;jmp 3
41: (X+C*A[J])/(C+1)→A[J];(Y+C*B[J])/(C+1)→B[J]
42: (Z+C*C[J])/(C+1)→C[J];next I
43: C+1→C;gto "DONE"
44: "CALMAG":
45: wrt 711,"AA1MN1MB1"
46: for I=1 to 8
47: wrt 711, "MP",S[I],"LMK";red 711,U,V
48: if A+B+C+D=Ø;V→F[I]
49: if V≠F[I];beep;dsp "FREQUENCY MISMATCH";stp
50: tn↑(U/1Ø)→U
51: if D=Ø;U→M[I];next I
52: uf D≠Ø;(U+D*M[I])/(D+1)→M[I];next I
53: wrt 711,"AAØ";D+1→D;gto "DONE"
54: "NOISE":
55: ent "TEMP",T;ent "DUT RESISTANCE",R
56: ent "CAL RESISTANCE",S;ent "DC CURRENT",U
57: gsb "LABEL"
58: for I=1 to 8;spc
59: √(A[I]*B[I]*C[I])→V;√(A[I+8]*B[I+8]*C[I+8])→W
60: √(A[I+16]*B[I+16]*C[I+16])→X
61: (V-W)/(X-W)→Y;M[I]/S/S→Z
62: Y*Z+4*1.38e-23*T/R→N
63: prt "SI=",N;fxd 1;prt "FREQ=",F[I];flt 3
64: next I
65: spc ; spc ;gto "DONE"
66: "CLEAR":
67: Ø→A→B→C→D
68: for I=1 to 8;Ø→F[I]→M[I];next I
```

```
69: for I=1 to 24;Ø→A[I]→B[I]→C[I];next I
70: gto "DONE"
71: "GET":
72: gsb "DATA"
73: if A+B+C+D=Ø;V→F[I]
74: if V#F[I];beep;dsp "FREQUENCY MISMATCH";stp
75: gsb "COH"
76: tn↑(X/1Ø)→X;tn↑(Y/1Ø)→Y;ret
77: "DATA":
78: wrt 711,"AA1MN1MB1"
79: wrt 711,MS[I]
80: wrt 711,"LMK";red 711,X,V
81: wrt 711,"AAØAB1LMK";red 711,Y,V
82: wrt 711,"ABØ";ret
83: "COH":
84: wrt 711,"LFM,",76ØØØ+dto(4*S[I]),",4";red 711
85: for J=1 to 4;rdb(731)→U;rdb(731)→Z
86: ior(rot(U,8),Z)→X[J];next J
87: wrt 711,"LFM,",77ØØØ+dtoS[I],",1";red 711
88: rdb(731)→X[2];rdb(731)→X[4]
89: wrt 711,"LFM,",75ØØØ+dtoS[I],",1";red 711
90: ior(rot(rdb(731),8),rdb(731))→X[5]
91: wrt 711,"LFM,",75200+dtoS[I],",1";red 711
92: ior(rot(rdb(731),8),rdb(731))→X[6]
93: wrt 711,"LFM,",77200+dtoS[I],",1";red 711
94: rdb(731)→X[7];rdb(731)→X[8]
95: X[1]*2↑(X[2]-15)→X[1]
96: X[3]*2↑(X[4]-15)→X[3]
97: X[5]*2↑(X[7]-15)→X[5]
98: X[6]*2↑(X[8]-15)→X[6]
99:(X[5]↑2+X[6]↑2)/X[1]/X[3]→Z
100: ret
101: "LABEL":
102: ent "Label",L$;spc :prt L$
103: prt "DCI=",U;prt "TEMP=",T
104: prt "DUT RES=",R;prt "CAL RES=",S
105: prt "# SETS=",A
106: ret
*19711
```

A.2 Wide-Band Filter Synthesizer

This program is written for the HP 9825 computer in conjunction with the HP 3582A spectrum analyzer. The high-frequency 4/5 of the FFT bins are averaged to synthesize a wide-band filter to use with the

radio frequency FFT system which utilizes a mixer just before the spectrum analyzer. Without the use of this program, the accuracy of a measurement is poor since the bandwidth is then very small compared with the frequency of interest. A bandwidth of 20 kHz can be generated by setting the frequency span on the 3582A to 25 kHz, although the program displays the filter output in normalized dBV/$\sqrt{Hz}$.

```
0: "Last 4/5'ths of display averager":
1: dim B[10],Y[256]
2: wrt 711,"LFM,77454,5"
3: red 711
4: for I=1 to 10;rdb*711)→B[I]
5: next I
6: wrt 711,"LSP";red 711,S
7: if B[3]>0;sfg 1
8: B[2]→H
9: if H>127;H-128→H
10: if H>63;H-64→H
11: if H>31;H-32→H
12: if H>15;H-16→H
13: if H>7;H-8→H
14: if H=0;250→B
15: if H>1;68.87→B
16: if H>3;166.6667→B
17: B[4]→H
18: if H>127;H-128→H
19: if H>63;H-64→H
20: if H>31;H-32→H
21: if H>15;H-16→H
22: if H>7;H-8→H
23: if H>3;H-4→H
24: if H>2;sfg 2
25: 128→N;if flg1;256→N
26: if not flg1;B/2→B
27: if flg2;256→N
28: wrt 711,"LDS"
29: red 711
30: for I=1 to N;red 731,Y[I]
31: next I
32: lcl 711
33: if flg2;128→N
34: 0→A;fxd 4
35: gsb "calc"
```

```
36: if flg2;X→Y;∅→X;128→A;gsb "calc"
37: if flg2;prt 2∅*log(Y/.8N),2∅log(X/.8N);end
38: prt 2∅log(X/.8N);end
39: "calc":
4∅: for I=A+N/5 to A+N;X+tn↑(Y[I]/2∅)/√(S/B)→X;next I
41: ret
*3∅119
```

REFERENCES

1. L. F. Eastman, R. Stall, D. Woodard, N. Dandekar, C. E. C. Wood, M. S. Shur, and K. Board, "Ballistic Electron Motion in GaAs at Room Temperature," Electron. Letters 16, 524 (1980).

2. M. S. Shur and L. F. Eastman, "Ballistic Transport in Semiconductor at Low Temperatures for Low-Power High-Speed Logic," IEEE Trans. Electron Devices ED-26, 1677 (1979).

3. J. R. Barker, D. K. Ferry, and H. L. Grubin, "On the Nature of Ballistic Transport in Short-Channel Semiconductor Devices," IEEE Electron Device Letters EDL-1, 209 (1980).

4. R. Zuleeg, "Possible Ballistic Effects in GaAs Current Limiters," IEEE Electron Device Letters EDL-1, 234 (1980).

5. M. S. Shur, "Ballistic Transport in a Semiconductor with Collisions," IEEE Trans. Electron Devices ED-28, 1120 (1981).

6. M. S. Shur and L. F. Eastman, "Near Ballistic Electron Transport in GaAs Devices at 77°K," Solid-State Electron. 24, 11 (1981).

7. J. J. Rosenberg, E. J. Yoffa, and M. I. Nathan, "Importance of Boundary Conditions to Conduction in Short Samples," IEEE Trans. Electron Devices ED-28, 941 (1981).

8. W. R. Frensley, "High-Frequency Effects of Ballistic Electron Transport in Semiconductors," IEEE Electron Device Letters EDL-1, 137 (1980).

9. A van der Ziel, M. S. Shur, K. Lee, T. Chen, and K. Amberiadis, "Carrier Distribution and Low-Field Resistance in Short n^+-n^--n^+ and n^+-p^--n^+ Structures," submitted to Solid-State Electron.

10. R. K. Cook and J. Frey, "Diffusion Effects and 'Ballistic Transport'," IEEE Trans. Electron Devices ED-28, 951 (1981).

11. Y. Awano, K. Tomizawa, N. Hashizume, and M. Kawashima, "Monte Carlo Particle Simulation of GaAs Submicron n^+-i-n^+ Diode," Electron. Letters 18, 133 (1982).

12. A. J. Holden and B. T. Debney, "Improved Theory of Ballistic Transport in One Dimension," Electron. Letters 18, 558 (1982).

13. T. C. Fry, "The Thermionic Current between Parallel Plane Electrodes; Velocities of Emission Distributed according to Maxwell's Law," Phys. Rev. 17, 441 (1921).

14. A. van der Ziel and G. Bosman, "Collision-Free Limit of Near-Thermal Noise in Short Solid-State Diodes," Physica Status Solidi a) 73, K93 (1982).

15. A. van der Ziel and G. Bosman, "Collision-Dominated Limit of Near-Thermal Noise in Short Solid-State Diodes," Physica Status Solidi (a), 73, K87 (1982).

16. F. N. Hooge, T. J. G. Kleinpenning, and L. K. van Damme, "Experimental Studies on 1/f Noise," Reports Progress in Physics 44, 479 (1971).

17. A. van der Ziel, "Flicker Noise in Electronic Devices," Advances in Electronics and Electron Physics 49, 225 (1979).

18. F. N. Hooge, "1/f Noise Is No Surface Effect," Phys. Letters A29, 139 (1969).

19. A. van der Ziel and C. M. Van Vliet, "Mobility-Fluctuation 1/f Noise in Nonuniform Nonlinear Samples and in Mesa Structures," Physica Status Solidi (a) 72, K53 (1982).

20. G. Bosman, R. J. J. Zijlstra, and A. D. van Rheenen, "Flicker Noise of Hot Electrons in Silicon at T = 78 K," Phys. Letters A78, 385 (1980).

21. T. M. Chen and A. van der Ziel, "Hanbury Brown-Twiss Type Circuit for Measuring Small Noise Signals," Proc. IEEE 53, 395 (1965).

22. L. D. Enochson and R. K. Otnes, Programming and Analysis for Digital Time Series Data, Shock and Vibration Center, Naval Research Laboratory, Washington, D.C., 201 (1968).

23. J. Kilmer, A. van der Ziel, and G. Bosman, "Presence of Mobility-Fluctuation 1/f Noise Identified in Silicon P^+NP Transistors," Solid-State Electron. 26, 71 (1983).

24. P. H. Handel, "Quantum Approach to 1/f Noise," Phys. Rev. A22, 745 (1980).

25. S. M. Sze, Physics of Semiconductor Devices, 2nd ed., Wiley-Interscience, New York, 851 (1981).

26. R. R. Schmidt, G. Bosman, A. van der Ziel, C. M. Van Vliet, and M. Hollis, "Nonlinear Characteristic of Short $n^+p^-n^+$ GaAs Devices," submitted to Solid-State Electron.

27. Th. G. van de Roer, "1/f Noise and Velocity Saturation in Punch-Through Diodes," Solid-State Electron. $\underline{23}$, 695 (1980).

28. A. van der Ziel, G. Bosman, and C. M. Van Vliet, "Predicted Nonlinear Characteristic of Short p^+-n^--p^+ GaAs Devices," internal report, Noise Research Laboratory, Electrical Engineering Department, University of Florida, Gainesville.

BIOGRAPHICAL SKETCH

Robert Roy Schmidt was born on November 11, 1952, in Edmonton, Alberta, Canada. Moving to the United States at the age of four, he lived in California and Washington, graduating from Redmond High School in 1970. He then attended the University of Washington, in Seattle, graduating in 1974 with a double major in physics and mathematics. In order to support his interest in music, for the next four years he worked as a professional bass guitarist, TV technician, residential carpenter, and electrician. Deciding to continue his education, he came to the University of Florida in January 1979 and began graduate study in electrical engineering. During this time he was employed in the Noise Research Laboratory as a graduate research assistant. He received the Master of Science in March 1981, writing a thesis on various transistor noise measurement systems from 0.06 Hz to 32 MHz. He is a member of Phi Kappa Phi Honor Society.

I certify that I have read this study and that in my opinion it conforms to acceptable standards of scholarly presentation and is fully adequate, in scope and quality, as a dissertation for the degree of Doctor of Philosophy.

C. M. Van Vliet, Chairperson
Professor of Electrical Engineering

I certify that I have read this study and that in my opinion it conforms to acceptable standards of scholarly presentation and is fully adequate, in scope and quality, as a dissertation for the degree of Doctor of Philosophy.

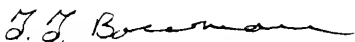E. R. Chenette, Cochairperson
Professor of Electrical Engineering

I certify that I have read this study and that in my opinion it conforms to acceptable standards of scholarly presentation and is fully adequate, in scope and quality, as a dissertation for the degree of Doctor of Philosophy.

G. Bosman
Assistant Professor of Electrical
    Engineering

I certify that I have read this study and that in my opinion it
conforms to acceptable standards of scholarly presentation and is fully
adequate, in scope and quality, as a dissertation for the degree of
Doctor of Philosophy.

A. D. Sutherland
Professor of Electrical Engineering

        I certify that I have read this study and that in my opinion it
conforms to acceptable standards of scholarly presentation and is fully
adequate, in scope and quality, as a dissertation for the degree of
Doctor of Philosophy.

T. T. Bowman
Associate Professor of Mathematics

This dissertation was submitted to the Graduate Faculty of the College
of Engineering and to the Graduate Council, and was accepted as partial
fulfillment of the requirements for the degree of Doctor of Philosophy.

April 1983

Dean, College of Engineering

Dean for Graduate Studies and Research